

UNIVERSITY OF READING

Department of Meteorology

A Simple Climate Model for Precipitation Response

Evgenios Koukouvagias

A dissertation submitted in partial fulfilment of the requirements for the
degree of Master of Science in Atmosphere, Ocean and Climate

August 13th 2012

Abstract

Radiative forcing (RF) is a useful concept for the quantification of global surface temperature anomalies, but is not so accurate for the evaluation of global precipitation changes. The reason is that the changes in precipitation rate depend on a variety of different climate change mechanisms and their effect on the atmospheric energy budget. Here a simple, zero-dimensional climate model is used following the methodology of Hansen et al. (1981), including a mixed-layer ocean coupled to a deep ocean by diffusion. The simple model uses time series for both anthropogenic and natural forcings at the top of the atmosphere.

The evaluation of precipitation changes is achieved by separating the precipitation response in two components; the fast atmospheric response to the RFs and the slow response to surface temperature anomalies. The precipitation response to both anthropogenic and natural radiative forcings is demonstrated, to determine the most significant climate change mechanisms. Also the outcomes of the simple climate model are compared with the results produced by complex climate models and observations. This comparison highlights possible changes in the simple climate model's parameters such as hydrological sensitivity and feedback parameter that improve agreement of the simple model with complex models and observations.

Analysis of the results shows that the climate change mechanisms which perturb atmospheric energy budget through the absorption of incoming solar radiation are dominated by the slow response to global surface temperature anomalies. This leads to the increase of precipitation rate. However, the positive radiative forcing of black carbon (absorbing aerosol) leads to increases in precipitation via the slow response but the atmospheric heating associated with solar absorption leads to decreased precipitation rate and this effect dominates. On the other hand, it is shown that the climate change mechanisms which perturb atmospheric budget through the scattering of incoming solar radiation are dominated by the surface temperature anomalies.

Acknowledgments

I wish to thank my supervisor, Dr Richard Allan of the Department of Meteorology for his invaluable support in all aspects of my work throughout this project. I am very grateful to Prof. Keith P. Shine for developing the spreadsheet model. I would also like to thank my family and my fiancé for their encouragement all these three months. My last, but by no mean the last appreciation goes to all of my friends especially to Rosemary Challen, Katie McLean and Seán Penston for keeping me entertained,.

Table of Contents

Abstract.....	i
Acknowledgments.....	ii
Chapter One: Introduction.....	1
1.1 Background and Motivation	1
1.2 Scope of this Dissertation	4
1.3 Climate Processes	4
1.3.1 Radiative forcings.....	5
1.3.2 Climate feedbacks.....	7
1.3.3 Precipitation.....	9
Chapter Two: Methodology	11
2.1. Model Setup.....	11
2.2 Feedback Parameter Y	12
2.3 Radiative Forcings at TOA	14
2.3.1 Well-mixed GHGs	14
2.3.2 Ozone	15
2.3.3 Tropospheric Aerosols	16
2.3.4 Aerosol indirect effect (cloud albedo)	17
2.3.5 Solar irradiance	17
2.3.6 Volcanic eruptions	19
2.4 Atmospheric Forcings	20
2.5 Evaluation of ratio R.....	21
2.6 Representation of atmospheric forcings	22
2.7 Precipitation Rate	24
Chapter Three: Experiments and Results.....	26
3.1 Precipitation Response using GHGs radiative forcings	26
3.2 Precipitation response using Aerosols radiative forcings.....	28
3.3 Precipitation Response using natural radiative forcings	32
3.4 Precipitation response using all radiative forcings	35
3.5 Precipitation response changing R value	39
3.6 Precipitation response changing feedback parameter	40
Chapter Four: Comparison with Complex models and Observations.....	42
4.1 Observations	42
4.1.1 Global-mean Precipitation Changes	43

4.1.2 Net radiative cooling.....	44
4.1.3 Comparison of Observations with Results.....	44
4.2 Temperature and precipitation response using complex climate models	46
4.2.1 Global-mean temperature anomaly	46
4.2.2 Global-mean precipitation rate	48
Chapter 5: Conclusions and Further Work.....	50
5.1 Conclusions	50
5.1.1 Experiments	50
5.1.3 Further experiments to explore and understand the uncertainty of the simple model	52
5.2 Future Work.....	53
Chapter 6: References.....	54
6.1 Bibliography	54
6.2 Web, Internet or Other Electronic References	62

Chapter One: Introduction

1.1 Background and Motivation

Climate incorporates the statistics of many meteorological elemental measurements such as temperature, humidity, atmospheric pressure, wind, and precipitation in a given region over long periods. Two major factors that affect climate include the sunlight energy and the atmosphere. The energy that heats the Earth is being supplied by sunlight, most of which passes through the atmosphere without being absorbed. The surface emits long wave infrared thermal radiation, which is mainly absorbed by the atmosphere and re-radiated both back to the space and towards the surface (Figure 1.1). This trapping of outgoing infrared radiation (greenhouse effect) leads to an enhancement of equilibrium temperature. This is accomplished by the various gases which compose the atmosphere (water vapour, CO₂, methane and others) and they are called greenhouse gases. The average global temperature is expected to be approximately 14°C. Research has shown that without the greenhouse effect, the global temperature would be 30°C cooler, making it uninhabitable to most forms of life (Schmidt et al. 2010).

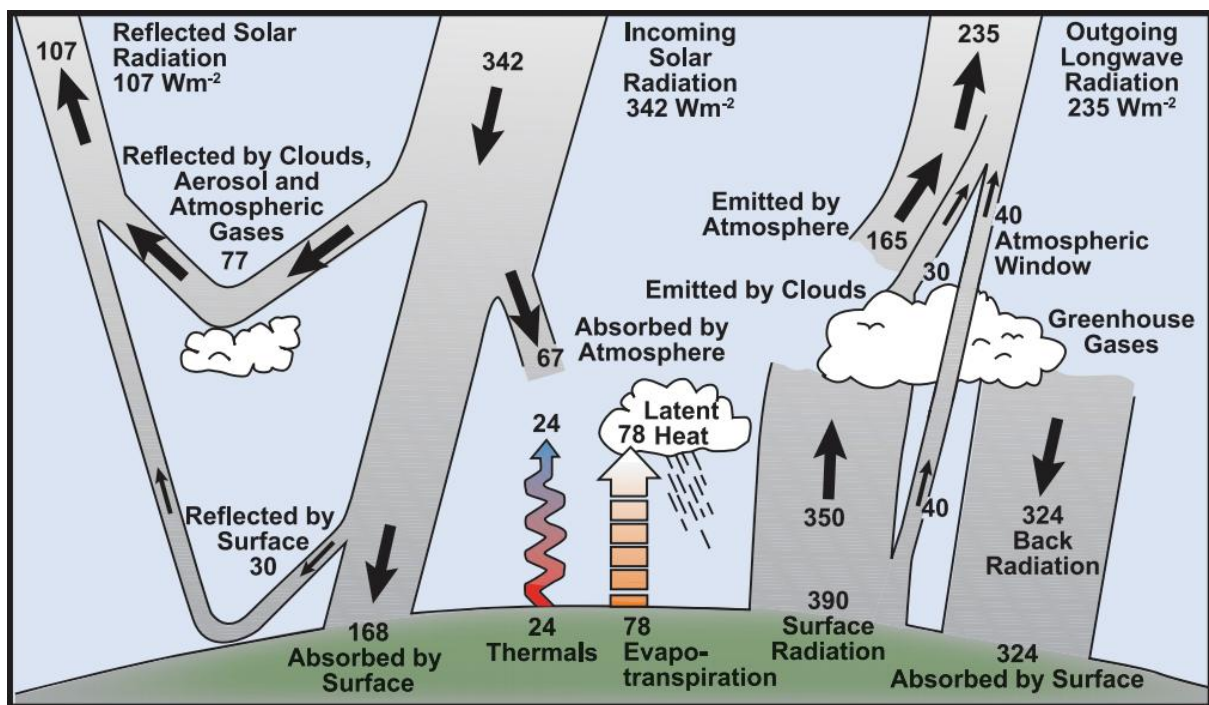


Figure 1.1: Schematic view of the Earth's energy balance. The incoming solar radiation absorbed by the Earth and atmosphere is balanced by outgoing infrared radiation. (Le Treut et al., 2007)

During the past decades, climate change has captured the interest of scientists and the public, considering the increased amount of evidence that demonstrate the impact of human activities on

the climate system, such as burning fossil fuels (like petrol and coal) and changing land use (such as chopping down forests for cattle grazing). The natural cycles such as El Nino, could not cause these long-term changes. Overwhelming evidence [e.g. Climate Change 2007-The Physical Science Basis, IPCC (2007)] show that atmospheric warming is caused by the increased concentrations of GHGs and absorbing aerosols in the last four decades.

Two major types of climate mechanism are recognised by scientist; forcings and feedbacks. Forcings are climate change mechanisms which do not react to changes in temperature. On the other hand, feedbacks respond to changes in temperature. The most important greenhouse gas is water vapour (feedback). The increase of water vapour (WV) concentration during the last five decades is caused due to the atmospheric warming (Trenberth et al., 2007). However, no extra reason other than increase in temperature is documented. This increase is described physically by the Clausius-Clapeyron relationship. CO₂ and methane are the most important forcings. Methane has a stronger greenhouse effect than CO₂ but it does not last as long as CO₂, which exists for about 100 years or more; also there is less methane than CO₂ in the atmosphere.

In addition to the greenhouse gas forcings, changes in the concentrations of aerosols can perturb the Earth's energy budget. They can be either solid or liquid particles which are suspended in the atmosphere. They have direct effect since they reflect solar radiation and absorb infrared radiation. Aerosols also modify cloud formation processes, increasing the number concentration of droplets and ice particles. Furthermore, they diminish the efficiency of warm clouds' precipitation and therefore, cause an indirect radiative forcing (RF). In addition to warm clouds, ice clouds can also be affected by aerosols. An important feature of aerosols is that they are short-lived in the atmosphere compared to the important greenhouse gases effecting the quantification of aerosol RF which is very complex. Many aerosols such as sulphates and secondary organics are not emitted directly but they are established in the atmosphere from gaseous precursors. There are also some types of aerosols that consist of particles whose physical properties, such as refractive index and size, have wide ranges. (Lead, 2005)

Climate theories are tested by numerical models which exploit quantitative methods to replicate the interactions of the atmosphere, oceans, land surface, and ice. Thus, they play an important role in environmental studies because of the time frame from years to thousands of years and the insufficient knowledge and complexity of the climate system. Models are used for a several purposes (e.g. projection of future climate) and they represent the real world. In accordance to the level of

simplification in a model, McGuffie and Henderson – Sellers (1997) produced a pyramid of climate model complexity. Complex models involve detailed description of physical processes including their equations. Furthermore, the complexity and their interaction often make interpretation difficult. Therefore, simpler models are required in climate change studies, like the one that will be presented in this dissertation.

Energetics play a significant role in global precipitation. Because of the small atmospheric heat capacity, there is a balance between the radiative cooling and latent and sensible heating; changes in the radiative cooling in particular offers a way to constrain future changes in latent heating and therefore precipitation (O’Gorman et al., 2011). Commonly, changes in all RFs, surface temperature and surface sensible heat flux should also be considered (O’Gorman et al., 2011). A diagram of the global atmospheric energy budget is portrayed in Figure 1.2.

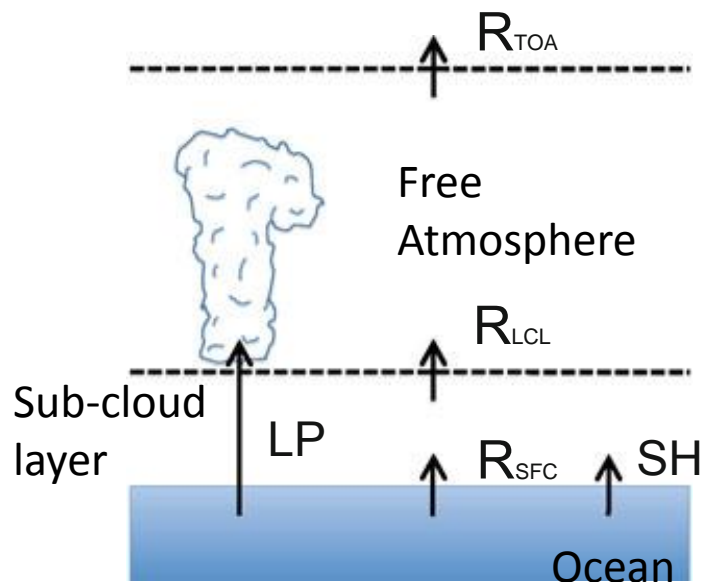


Figure 1.2: Illustration of the energy budgets of global atmospheric energy budget, as defined in the text; LCL is the elevated condensation level. (Takahashi, 2009)

In the above diagram, L is the latent heat¹ of condensation which is presumed as constant, P is the precipitation rate, R represents the net radiation flux and SH is the surface sensible heat flux which is rather large on average and is neglected in this dissertation. Heating below the LCL is balanced by changes in SH , but for simplicity only total R is considered. According to figure 1.2, the perturbation budget between two climates can be described as:

$$L\Delta P = \Delta R_{TOA} - \Delta R_{SFC} - \Delta SH \quad (1)$$

¹ Latent heat is a characteristic amount of energy absorbed or released by a substance during a change in its physical state that occurs without changing its temperature.

The changes in sensible heat flux are considered negligible in this project; therefore precipitation changes are linked to changes in the atmospheric radiative cooling. Commonly, the variations in all RF terms and global surface temperature anomalies must be taken into account.

1.2 Scope of this Dissertation

Recent research (Andrews et al., 2010) highlights that global precipitation is related to the surface temperature response and the RF. In this project, a framework is cultivated by a simplified excel spread-sheet climate model. The aim is to determine fast precipitation responses to each RF and the inclusion of these responses in the climate model. Past and present precipitation changes are simulated with the model and experiments are performed to assess the precipitation sensitivity to a variety of RFs.

The next section presents an introduction to the climate processes and feedbacks that govern climate. A general description of the used climate model is established in chapter 2, followed by a discrete description of the methods which have been used. Chapter 3 starts with the results from the climate model, using all the given parameters together. The model parameters are being set by Andrews et.al (2010). Then, an analytical discussion about the results and the uncertainties involved in the model will be presented. Chapter 4 deals with the comparison of the estimated global precipitation change with the actual observations from 1990 to 2010 and detailed climate models simulations from 1850 to 2005. The outcomes from the climate model are compared to the observations graphically and statistically. Description of the sources and characteristics of the major RFs and detailed discussion of model sensitivity to uncertainty in model inputs will also be demonstrated.

1.3 Climate Processes

The climate system consists of five key parts: the atmosphere, the hydrosphere, the cryosphere, the land surface, and the biosphere driven by external forcing mechanisms including Sun, human activities, and volcanic eruptions which emit a great amount of greenhouse gases and aerosols (IPCC, 2001: Climate Change 2001: The Scientific Basis). The interaction of these major components determines the Earth's surface climate (Harvey, 2000). Figure 1.3 shows the major components of climate systems. Changes in the external forcing mechanisms affect the balance between the incoming solar and outgoing long wave radiation. This influence is quantified using the metric, RF to

the climate system (IPCC, 2001: Climate Change 2001: The Scientific Basis). Perturbations to the external forcings are considered to be the sources of climate change (IPCC, 1990).

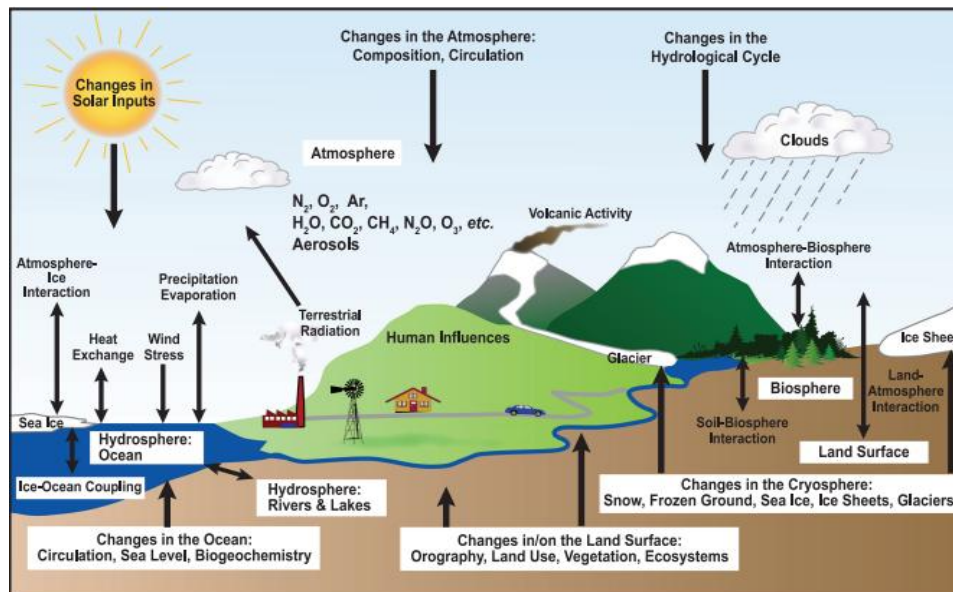


Figure 1.3: Schematic view of the components of the global climate system (bold), their developments, and interactions (thin arrows) and some traits that may change (bold arrows). (Le Treut et al., 2007)

1.3.1 Radiative forcings

The impact of external forcing mechanisms on climate is determined by its radiative forcing. The word radiative describes the perturbation on the balance between the absorbed solar and the outgoing long wave radiation. The term forcing arises because the Earth's radiative balance is driven away from its normal state. RF is defined as the "rate of energy change per unit area of the globe as measured at the top of the atmosphere (TOA)" and is expressed in units of 'Watts per square meter' (Forster et al., 2007). The energy of the Earth-atmosphere system can be enlarged, forcing to a warming of the system (positive RF) or decreased, leading to a cooling of the system (negative RF). (Forster et al., 2007)

Rising concentrations of greenhouse gases lead to a positive RF because each gas absorbs outgoing long wave radiation in the atmosphere (Figure 1.4). It is observed that increases in CO_2 have triggered the largest forcing over the last decades. In contrast to greenhouse gases, aerosols influence RF directly through reflection and absorption of solar and infrared radiation in the atmosphere. There are two categories of aerosols: absorbing aerosols which generate positive forcings and scattering aerosols that cause negative RF. Their direct RF is negative but they can also

produce an indirectly negative RF through the changes of cloud albedo (Figure 1.4). (Forster et al., 2007)

During the industrial era, human activities caused changes in croplands and forests. They also altered the reflective properties of ice and snow. Therefore, more solar radiation is reflected by the Earth's surface and a negative forcing is ensued by this change. Another RF term is the condensation trails left behind jet aircrafts known as contrails. Contrails are formed when the hot humid air from jet engines get mixed with the cooler environmental air. The mixing is a result of turbulence produced by the engine exhaust (Minnis et al., 2004). They are forms of cirrus cloud that reflect solar radiation and capture infrared radiation, causing a small positive RF (Forster et al., 2007). During the day, the effect of blocked incoming radiation is likely to offset that of trapped heat, thus cooling the atmosphere. On the other hand, the atmosphere is warmed during the night due to the trapped infrared radiation (Haywood et al., 2009).

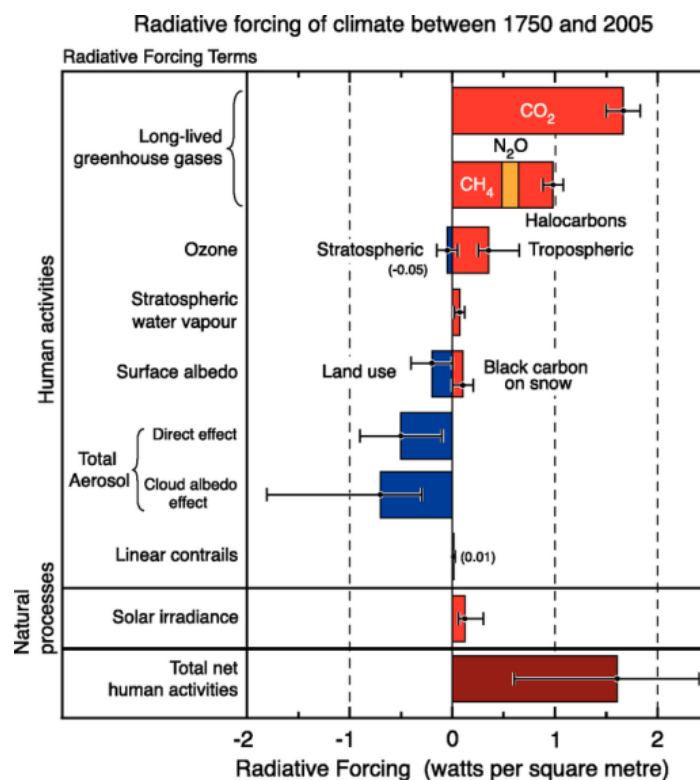


Figure 1.4: Representation of all RF agents and their RFs. The RF terms are separated in two categories; human activities and natural processes, as described in the text (Forster et al., 2007)

In contrast, natural forcings include changes in solar irradiance and volcanic eruptions. A gradual increase of solar output was observed in the industrial era (mostly in early 20th century) and along

with the cyclic changes in solar radiation, is causing a small positive RF (Figure 4). Solar energy directly influences the heating of the climate system and indirectly affects the great quantity of some GHGs such as stratospheric ozone. Volcanic eruptions can cause a short-lived negative forcing of two to three years through the temporary increase of sulphate aerosol in the stratosphere but it is a standard practice to calculate their RF at the TOA after allowing the stratosphere to adjust. The last major eruption was in 1991 (Mt. Pinatubo). A summary of the principal constituents of the RF of climate change is represented in Figure 1.4. (Forster et al., 2007)

1.3.2 Climate feedbacks

A perturbation in climate affects the climate further. This effect is called climate feedback. Climate Feedbacks are divided in to two categories, positive and negative. Negative feedback adapts the dominant change in climate. For example, under global warming, negative feedback would generate a cooling effect, offsetting the initial change. On the other hand, Positive feedback amplifies the initial climate change. Therefore, in a warmer atmosphere it would cause further heating. (Randall et al., 2007)

Climate feedbacks play a significant part in climate change studies. In a warm climate, the apparent feedback is generated by the heated surface itself. According to Stephan-Boltzmann law which claims that the total radiant heat energy released from a surface is comparative to the fourth power of its absolute temperature, an increase in the surface temperature will enhance the amount of the outgoing long wave radiation, which in sequence will diminish the intensity of surface heating. This process is called radiative damping (Harvey, 2000). On the contrary, the amount of long wave radiation will be less if there is a negative forcing which dampens the surface temperature. Consequently, the cooling of the surface will be diminished. The surface proceeds in order to reduce the initial perturbation, a negative feedback.

According to the Clausius Clapeyron relationship, the vapour pressure increases as the temperature increases. Therefore, if air becomes warmer, its capacity to hold moisture rises. Climate studies show an atmospheric warming in the last decades (Wentz & Schabel et al., 2000). Subsequently, the amount of water vapour increased, due to the increase of atmospheric holding capacity and the evaporation from water bodies and wetlands (Raval and Ramathan, 1989). Water vapour supports the Earth to absorb more sunlight energy. Hence, an increase of atmospheric water vapour concentration is observed under global warming, which in turn warms the climate further, a classic

positive feedback (Figure 1.5). Its effect depends on its latitudinal and vertical distributions as well as the lapse rate feedback (Stocker et al., 2001).

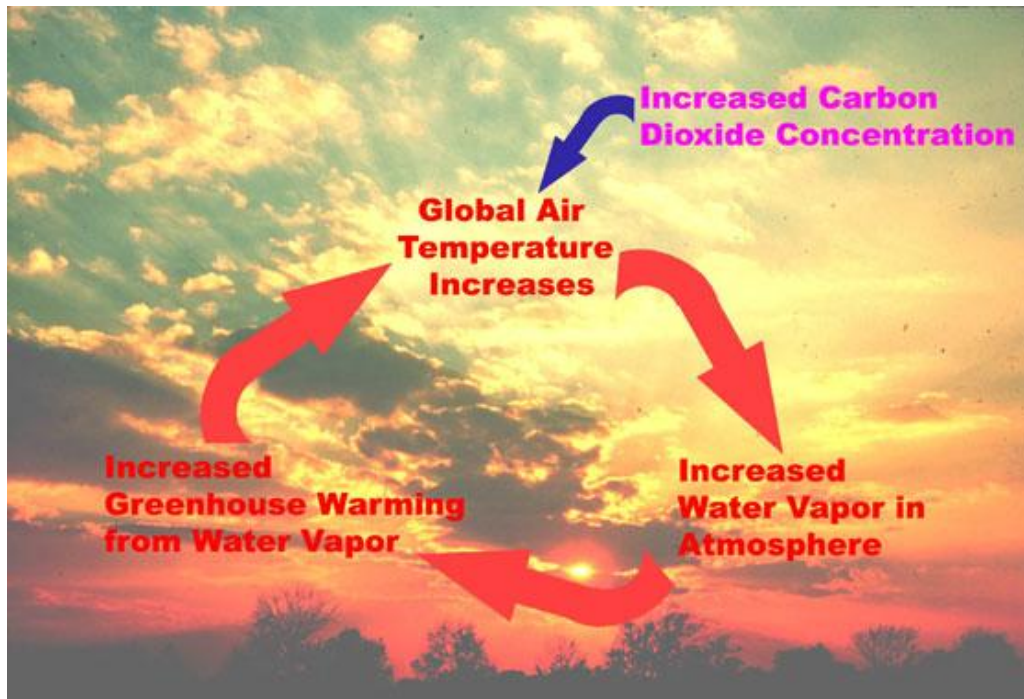


Figure 1.5: Illustration of positive water vapour feedback. Increasing CO₂ concentration, the global temperature increases and leads to the enhancement of water vapour amount in the atmosphere, due to the increased evaporation and the ability of warmer air to hold more water. The enhancement of water vapour amount further increases greenhouse warming. (NASA, 2012)

Albedo is the quantity of light reflected by a surface. Therefore, snow or sand, will reflect more sunlight back out to space than a surface with low albedo where more heat and energy will be absorbed. Global warming is reducing global ice and snow cover which reflect more sunlight than land or ocean. Thus, ice and snow melting leads to further global warming as more sunlight is being absorbed (positive ice-albedo feedback) (Shine et al., 1984).

The way climate change influences clouds could produce a positive or negative feedback. There is limited understanding from some climate models for reduced stratocumulus clouds in a warming climate, leading to a net positive feedback. Many also observe the effect on high clouds, such as cirrus (Bony et al., 2006). Cirrus clouds reflect sunlight similarly to stratocumulus, but they are more powerful maintaining heat radiating away from the Earth's surface. Therefore, in contrast to stratocumulus clouds, increases in cirrus will cause global warming, while reductions will cause cooling. More researches into this area will advance in understanding as well as allow scientists, researchers, and the public to improve confidence in climate projections (Zelinka and Hartmann et al., 2010).

1.3.3 Precipitation

The energetic constraint explained above was also examined comprehensively by Mitchell et al. (1987). More recently, there has been significant progress on evaluation and understanding of the response of precipitation to climate change such as the influence of climate feedbacks (e.g., Stephens and Ellis 2008; Previdi 2010) and how precipitation response adjusts according to different RF agents (e.g., Andrews et al. 2010).

The energetic constraint does not propose that the water vapour in the atmosphere determines the global-mean precipitation, even if water vapour does play a substantial radiative role (Allan, 2009). However, precipitation extremes and intensity are directly influenced by changes in water vapour concentrations (Trenberth et al., 2003). The energetic constraint on global-mean precipitation is usually determined as radiative constraint in which latent heat release is in balance with the radiative cooling.

Precipitation is a common term which describes all forms of liquid falling from the clouds. Precipitation is sporadic and is formed by the condensation of water vapour, usually in rising air that expands and therefore cools. This event can come from a variety of different aspects such as rise of air over mountains, warm air riding over cooler air (warm front), and colder air pushing beneath warmer air (cold front). Thus, changes in any of these features modify precipitation. (Anagnostou et al., 2004)

The enhancement of the greenhouse gases has as a consequence the increase of evaporation, given that adequate surface moisture is obtainable. Therefore, surface moisture behaves as an 'air conditioner', because heat which is necessary for the process of vaporisation moistens the air instead of warming it (Randall et al., 2007). This implies that summers are likely to be either warm and dry or cool and wet. However, during the winter over northern continents, the largest amounts of precipitation are related to higher temperatures, due to the greater water holding capacity of the atmosphere rises in the warmer conditions (Hegerl et al., 2007).

Warming intensifies the frequency and severity of droughts globally (Figure 1.6). *"However, Clausius-Clapeyron relation establishes that the water-holding capacity of the atmosphere increases by about 7% for every 1°C rise in temperature"* (Randall et al., 2007). Over the 20th century, water vapour increased by approximately 5% in the atmosphere over the ocean (Randall et al., 2007). Because precipitation is originated mainly by weather systems that feed on the water vapour deposited in

the atmosphere; this raises precipitation intensity and the risk of heavy rain and snow events (Randall et al., 2007). The warmer climate thus, enlarges risks of both droughts in non-rainy areas and floods in rainy regions but at different times and/or places. For example, widespread floods occurred in the summer of 2002 in Europe but a year later record-breaking heat waves and drought were documented (Robine, 2008).

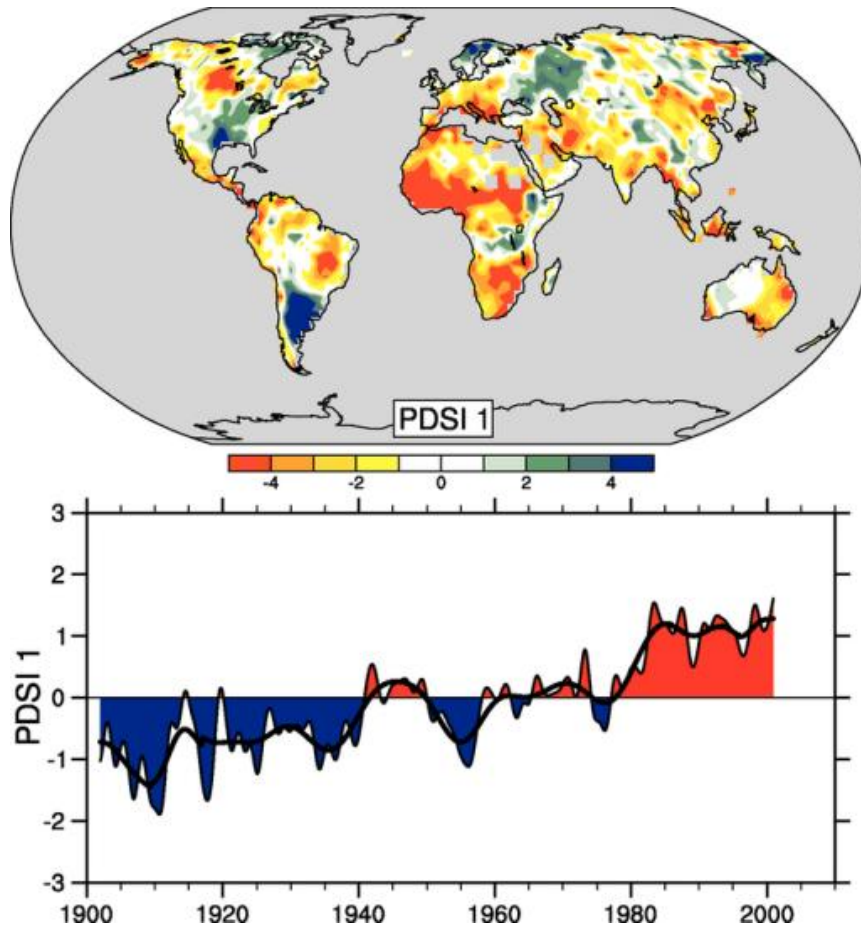


Figure 1.6: The most important spatial pattern (top) of the monthly Palmer Drought Severity Index (PDSI) for 1900 to 2002. (Bates et al., 2008)

In regions with strong aerosol pollution, the rate of evaporation is declined. Hereafter, even as the potential for heavier precipitation outcomes from more water vapour amounts, the duration and frequency of events may be shortened, as it takes longer to restore the atmosphere with water vapour (Hegerl et al., 2007).

Chapter Two: Methodology

2.1. Model Setup

A simple global mean, zero-dimensional, climate model is used following the methodology of Hansen et al. (1981). It includes a mixed-layer ocean (typically 100 meters deep) coupled to a deep ocean by diffusion (Figure 2.1). It exploits the time series of both natural and anthropogenic forcings from GISS and the MAGICC model equivalently. Anthropogenic forcings demonstrate data for well-mixed GHGs (Hansen and Sato (2004) and Montzka et al., 1999), trace gases (Montzka et al., 1999), and tropospheric aerosols (Hansen et al., 2007). On the other hand, natural forcings consist of data for solar irradiance (Lean, 2000) and volcanic eruptions from 1850 to 2010 (Sato et al., 1993). All anthropogenic forcings are without carbon cycle feedbacks. The data are relative to 1750, while some values from 1995 were obtained by simple extrapolation. The results, as an anomaly from 1961-1990 means, are compared with the HadCRUT3v global temperature dataset created by the Hadley Centre and the Climatic Research Unit at UEA (Brohan et al. 2006). It is also shown as absolute temperature change since 1850 and compared against the equilibrium change to give an idea of the “hidden” warming in the system.

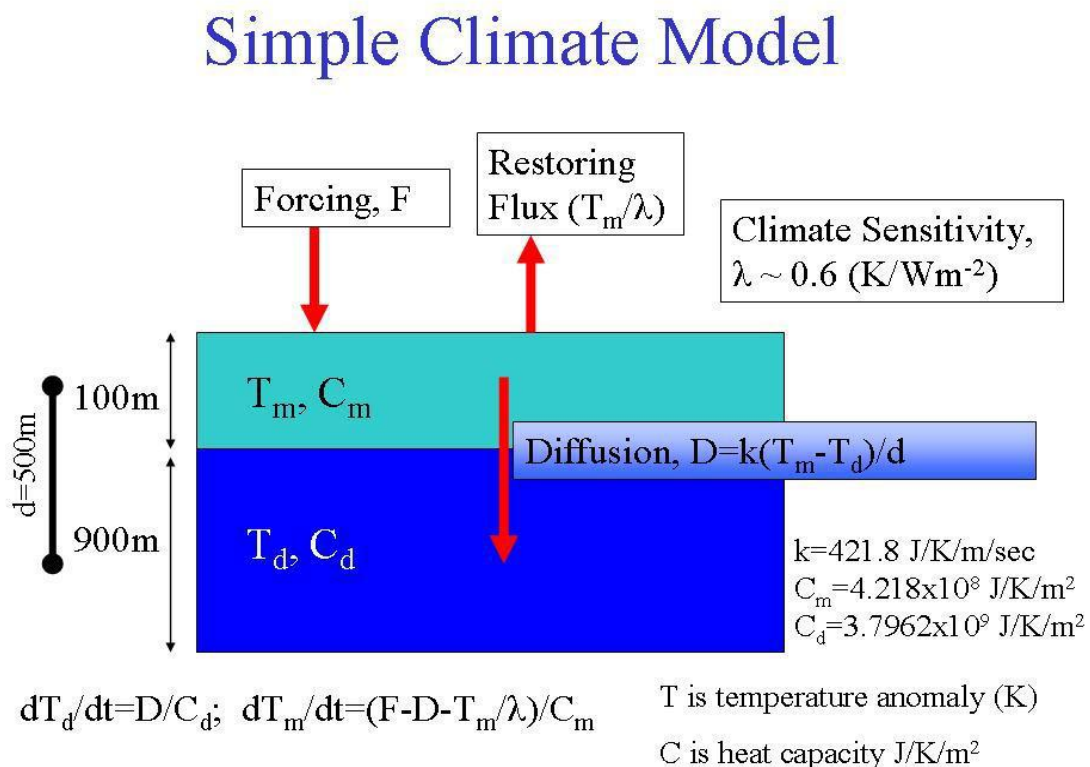


Figure 2.1: Illustration of a simple global mean, zero-dimensional model which is using the methodology of Hansen et al. 1981.

The understanding of the steady-state global temperature change ΔT as a result of the change in the external heating ΔQ can be determined in terms of the extremely simple “zero-dimensional” climate model,

$$\Delta T = \frac{\Delta F}{Y} \quad (2)$$

The feedback parameter Y (in Figure 2.1 is demonstrated as $1/\lambda$) evaluates the change of outgoing thermal and reflected solar radiation at the top of the atmosphere; it has the likely value $Y = 1.7 \pm 0.8 \frac{W}{m^2K}$ (NAS, 1979) and is further clarified in Section 2.2. ΔF represents the change of radiative forcing which is the mechanism that causes Q to change instantaneously. The time-dependent generalization of (2) is,

$$\frac{CdT}{dt} + Y\Delta T = \Delta F - D \quad (3)$$

where C is the heat capacity of the atmosphere-ocean climate system. Climate system has a variety of thermal reservoirs with differing heat capacities that cause a conceptual difficulty in the operation of Eq.3. Therefore, the value of heat capacity is governed by the chosen time scale in the climate model. On time scales of years to decades, the heat capacities of both mixed layer and intermediate layer waters of the oceans are required. The temperature multiplied by the feedback parameter is determined as the weighted average of the atmospheric and ocean surface temperatures. Since, both atmospheric and ocean surface temperatures closely follow each other, this term is interchangeable with the atmospheric temperatures. All the values of the parameters that are being used in the simple climate model are demonstrated in Table 1.

Table 1: Representation of all parameters which are used in the simple, global-mean, zero-dimensional, climate model.

Feedback Parameter (Y)	$1.30 \text{ Wm}^{-2}\text{K}^{-1}$
Climate Sensitivity ($\lambda=1/Y$)	$0.77 \text{ KW}^{-1}\text{m}^2$
Diffusivity (D)	$0.00010 \text{ m}^2/\text{s}$
Mixed Heat Capacity (C_m)	$42,18 \times 10^7 \text{ JK}^{-1}\text{m}^{-2}$
Deep Heat Capacity (C_d)	$37,962 \times 10^8 \text{ JK}^{-1}\text{m}^{-2}$

2.2 Feedback Parameter Y

The climate feedback parameter used is a net value for all the given RF. Since each forcing is associated with a unique climate sensitivity with an error, the value of feedback parameter (Y) is difficult to determine. To think about what role Y plays in the model, the equations for a simple climate model shall be examined.

As shown in Eq.2, a higher value of Y will yield a smaller equilibrium temperature (and equilibrium climate sensitivity). This is justly as a positive contribution to Y is a negative feedback. This model tells nothing about how quickly the system responds.

The transient climate change model is,

$$\Delta T(t) = e^{-Yt/c_s} \int_0^t \frac{\Delta F(t')}{c_s} e^{\frac{Yt'}{c_s}} dt' \quad , \text{ where } C_s \text{ is the heat capacity per unit area.} \quad (4)$$

It is a generalised version of the simple model of equilibrium climate change considering time dependency.

In order to discover what role Y plays in the model and what uncertainties are associated with it, a new simple forcing is being added and the model is run with only this forcing turned on, varying the value of feedback parameter between 1.3 and 3.3 $\text{Wm}^{-2}\text{K}^{-1}$ (Figure 2.2) to see what happens to the shape of the model and the equilibrium temperature. The simple forcing has been chosen to be equal to zero apart from a number of years when it is equal to 1.

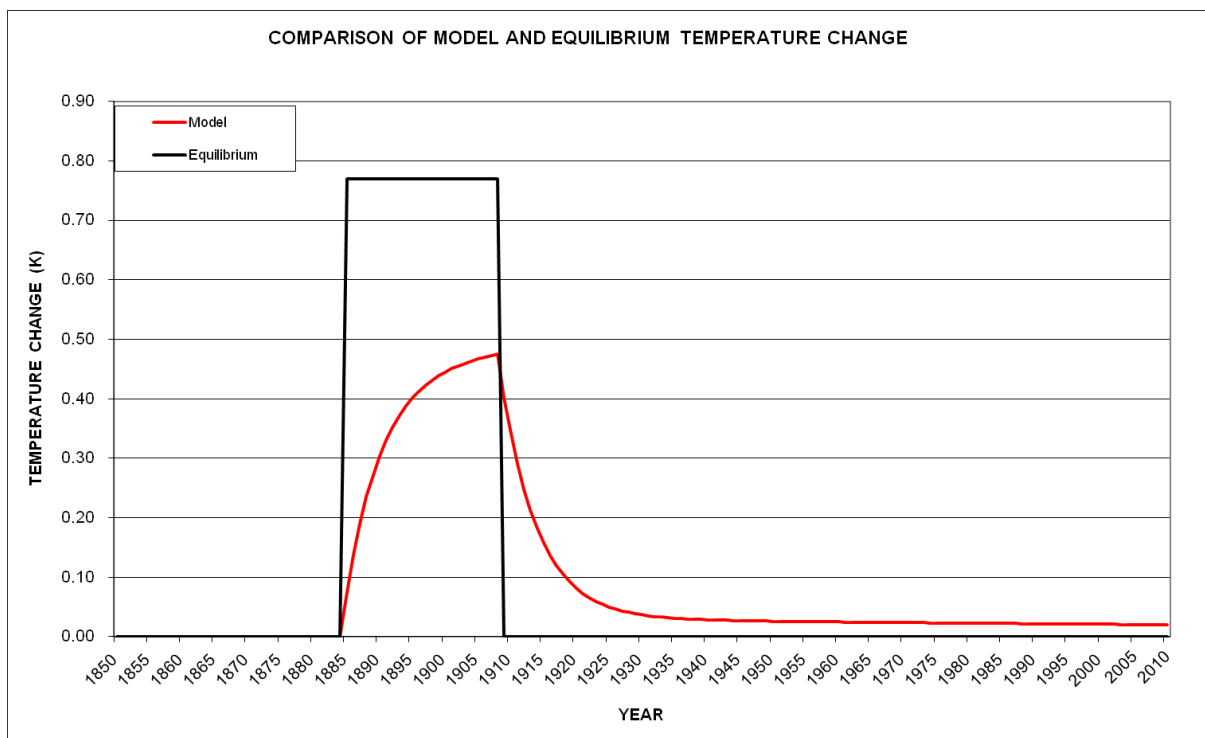


Figure 2.2: Comparison of model and equilibrium temperature change for the simple global mean, zero-dimensional, climate model with a feedback parameter, $Y=1.3 \text{ Wm}^{-2}\text{K}^{-1}$. The model gets closer to equilibrium temperature change and at a faster rate for a feedback parameter, $Y=3.3 \text{ Wm}^{-2}\text{K}^{-1}$.

When Y is enhanced, the model gets closer to equilibrium temperature change at a faster rate than with a smaller value of Y . The maximum temperature change of the model is lower than using a small value of Y . This can also be explained mathematically from the equation for the transient climate model (Eq. 4). As the feedback parameter affects how quickly the model reaches the equilibrium value, uncertainty in its value will affect any future climate change projections. If a larger value of Y is used incorrectly the model will predict a much faster warming of the planet than is realistic. When Y is altered in this model, it does not take into account how the climate sensitivity may change differently over time for different RFs, adding more uncertainty into the projections of future climate change. The above result can also be depicted by turning on all the RFs and comparing model and equilibrium change, using the two different feedback parameters.

2.3 Radiative Forcings at TOA

The RFs at the TOA were described in the climate model. The RFs which are included in the climate model and drive the simulated climate change arise from well-mixed greenhouse gases, stratospheric and tropospheric ozone, tropospheric aerosols, specifically, sulphates, biomass burning, black carbon, volcanic aerosols, solar irradiance, and cloud albedo. In the last century, the largest RFs are for GHGs and aerosols, comprising the aerosol indirect effect. Ozone global forcing and uncertain solar forcing are important on the century timescale. Volcanic effects are large but short-lived of about two to three years through the temporary increase of sulphate aerosol in the stratosphere.

2.3.1 Well-mixed GHGs

The changes of well-mixed GHGs concentrations can be assumed as globally. According to Hansen and Sato (2004), these values were taken from a suitable area allowing of in situ and ice core measurements at particular locations. In addition, trace gases (stratospheric and atmospheric ozone) measurements are assessed by Montzka et al. (1999). Then, a model radiation code is being used to convert the gas amounts to forcings, for IPCC and alternative scenarios. The resulting forcings and the growth rate of forcings are illustrated in Figure 2.3a and 2.3b respectively. The adjusted forcings from 1880 to 2010 for all well-mixed greenhouse gases is 2.65 W/m^2 .

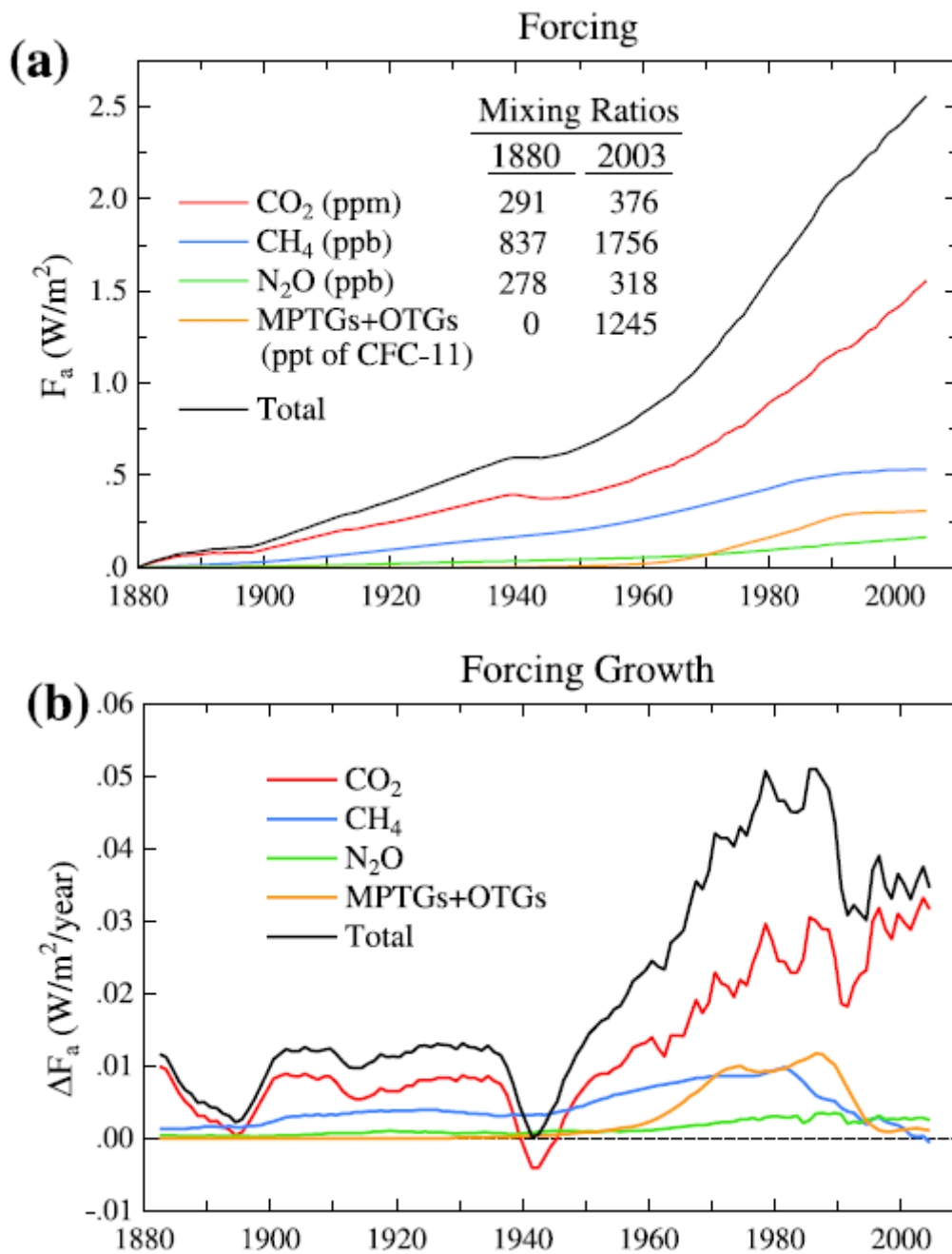


Figure 2.3: Climate forcing (W/m^2) and its annual changes (W/m^2 per year) for observed 1880–2010 greenhouse gas changes as presented by Hansen and Sato(2004). MPTGs and OTGs are Montreal Protocol trace gases and other trace gases (Hansen and Sato 2004).

The growth rate dropped from $5 \text{ W}/\text{m}^2/\text{century}$ 25 years ago to $3.5 \text{ W}/\text{m}^2/\text{century}$ more recently due to the decrease of Montreal Protocol trace gases and methane concentrations.

2.3.2 Ozone

Ozone is the major, short-lived, and non-well-mixed GHG. Ozone changes include both an increase of tropospheric ozone and stratospheric ozone reduction in recent decades. The tropospheric

historical ozone change in the climate model is given by a chemistry climate model (Shindell et al. 2003) forced by recommended changes of ozone forerunner emissions and climate conditions. Stratospheric ozone alteration is mainly based in the observational studies of Randel and Wu (1999). The decrease of stratospheric ozone influences tropospheric ozone by inferring ozone tendencies in the Antarctic all the way to the surface and decreasing ozone in Arctic troposphere.

2.3.3 Tropospheric Aerosols

Aerosols are highly uncertain causing difficulties in the understanding of climate change. Its magnitude will remain approximately implied through climate change studies and understanding of climate sensitivity. The climate model unambiguously permitted aerosol forcing and the climate response function to be free variables. Observed temperature anomalies and ocean heat uptake are employed in order to determine the aerosol RF and response function that acquiesce with observations.

The time series of aerosol RF produced by the simple climate model is illustrated in Figure 2.4. Aerosol modeling (Koch, 2001) was used to construct the RF for 18-80-1990, introduced by Hansen et al. (2007). The aerosol modelling is using aerosol emissions from fuel use statistics and incorporating historical variations in fossil fuel technologies (Novakov et al., 2003). Aerosol forcing, after 1990, is anticipated to be half as large and opposite in sign of the GHG forcing. This inaccurate assumption attempts to represent the modest decrease of aerosol concentration in developed nations and increased aerosol amount in emerging nations.

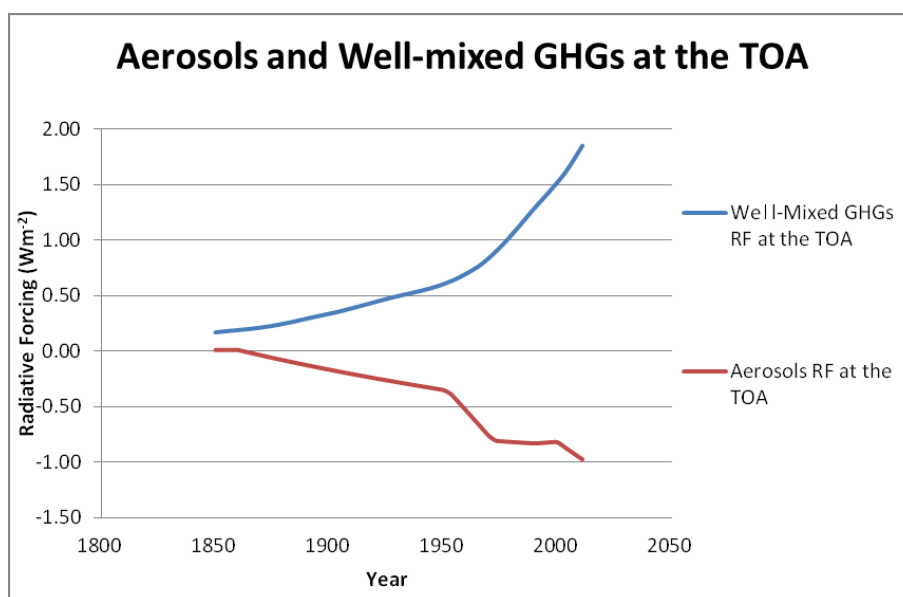


Figure 2.4: Illustration of aerosol forcing employed by the climate model, including both direct and indirect effects.

The resulting aerosol forcing in 2010 is -1 W/m^2 and does not exceed IPCC (2007), including all indirect effects. For instance, a variety of models (e.g. Scott and Forest, 2007 and Figure 2.5 Hansen et al., 2007) determined aerosol forcings between -0.4 to -1.1 W/m^2 . Therefore, the model agrees with observed temperature change because the ocean-atmosphere coupled models have a slower response than the real world, mixing heat into the deep ocean or model feedbacks are inaccurate (Kiehl et al., 2007).

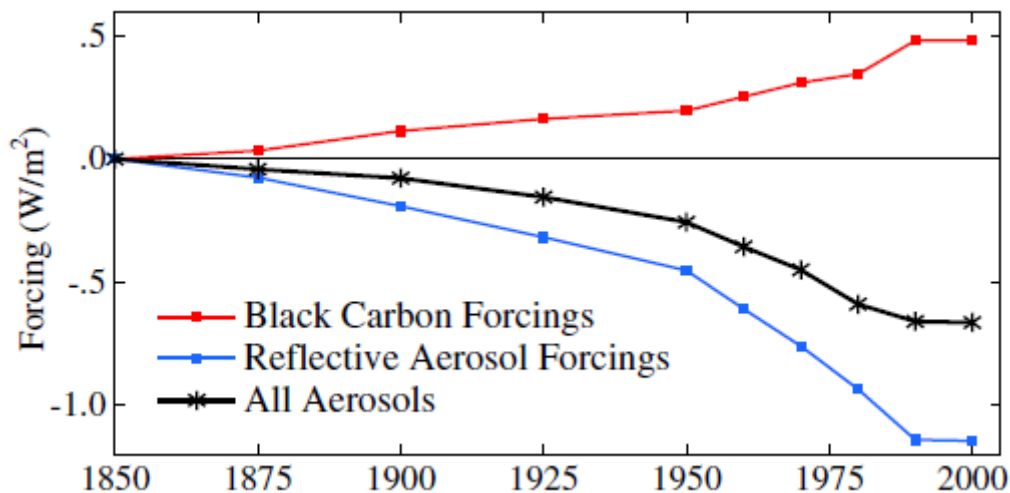


Figure 2.5: Time dependence of aerosol forcings described by GISS modelE. (Hansen et al., 2007)

2.3.4 Aerosol indirect effect (cloud albedo)

Cloud albedo is taken into account in the climate model, i.e., a parameterization according to the realistic effects on the concentration of cloud droplets (Menon and Del Genio, 2006). Along with empirical evidence, it is maintained that the significance of cloud albedo is generated by the changes in cloud cover and that the mean value of indirect aerosol RF is -1 W/m^2 , but highly uncertain (at least 50%).

The global mean value of indirect aerosol forcing which is described in a variety of empirical studies should be regarded as an estimate for the entire aerosol indirect effect, as the cloud albedo is not taken explicitly into account. The indirect forcing which is employed in the climate model is smaller (-0.8 W/m^2) than in most models revised by Lohmann and Feichter (2005), yet recent studies recommend even smaller values (e.g. Penner et al., 2006, Quaas and Boucher 2005).

2.3.5 Solar irradiance

Satellites evaluated solar irradiance since 1979. Time series of solar irradiance is illustrated in Figure 2.6, based on Lean (2000). The permanence of the recent prolonged solar minimum shows that solar

minimum is possibly a compelling force for cooling. The amplitude of solar irradiance variability is approximately 1.5 Wm^{-2} , but because the amount that is being absorbed by the Earth is only 240 Wm^{-2} (global average), the amplitude of solar forcing is roughly 0.25 Wm^{-2} . In comparison with the human-made GHG forcing, solar irradiance forcing is trivial, but because of the efficiency of solar variability on near-term climate change is more suitable to assess solar forcing with Earth's current energy imbalance which is 0.6 Wm^{-2} (Loeb et al., 2012). Therefore, the solar forcing is not negligible.

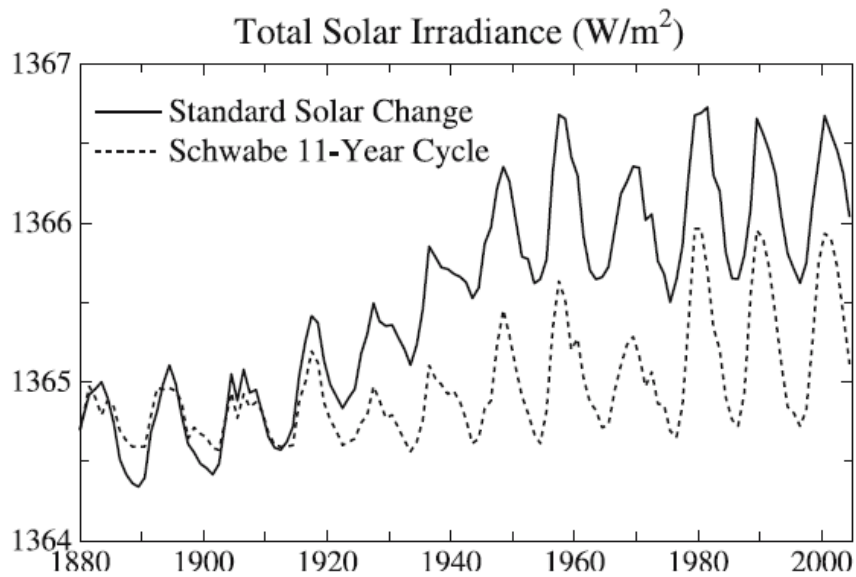


Figure 2.6: The standard solar variability according to Lean (2000) based on observations of solar irradiance since 1979 and solar proxy variables in prior years. Dotted curve illustrates the alternative solar forcing using only the Schwabe 11-year variability from Lean et al. (2002)

The direct solar forcing is decreasing due to the absence of the indirect solar forcing on ozone (Hansen et al. 1997b). Shindell et al. (2001) argued that the indirect effect of solar irradiance on ozone is trivial, but climate change in particular regions is triggered possibly by important dynamical feedbacks (Shindell et al., 2001).

Solar irradiance forcing is compared with a solar irradiance scenario by Lean et al. (2002). The scenario involves only the Schwabe 11-year solar cycle (dotted curve in Figure 2.6), questioning the earlier indirect long-term changes due to the comprehension that secular enhancements in cosmogenic and geomagnetic substitutions of solar activity do not certainly infer comparable secular trends of solar irradiance (Hansen et al., 2007).

2.3.6 Volcanic eruptions

Hansen et al. (2002) built a volcanic aerosols data set from 1850 to 2000, employing available satellite images and ground-based observations (Sato et al., 1993). The global mean RF estimated using the Sato et al. (1993) data generates a peak in RF of approximately -3 Wm^{-2} (optical depth of about 0.16) for the large 1883 and 1991 eruptions of Krakatau and Mt. Pinatubo respectively. In addition, intense El Chichón and Agung eruptions (Hansen et al., 2002) produced a negative RF of about -2 Wm^{-2} .

Ammann et al. (2003) produced a data set of total aerosol optical depth since 1890 excluding the Krakatau eruption. This figure is established using empirical approximations of atmospheric loadings and uses a fixed aerosol effective radius ($0.42 \mu\text{m}$) in order to calculate optical properties. However, the RFs estimated by Ammann et al. (2003) is roughly 20 to 30% larger than these evaluated by Sato et al. (1993). Further improvement of data sets is required as only some of the aerosols are well computed. This embraces improved estimations of the aerosol size parameters (Bingen et al., 2004) and comparison of data from different satellites plugging also data to gap-dates (Randall et al., 2001). Optical depths time series of stratospheric sulphate aerosols from Sato et al. (1993) and Ammann et al. (2003) are illustrated in Figure 2.7.

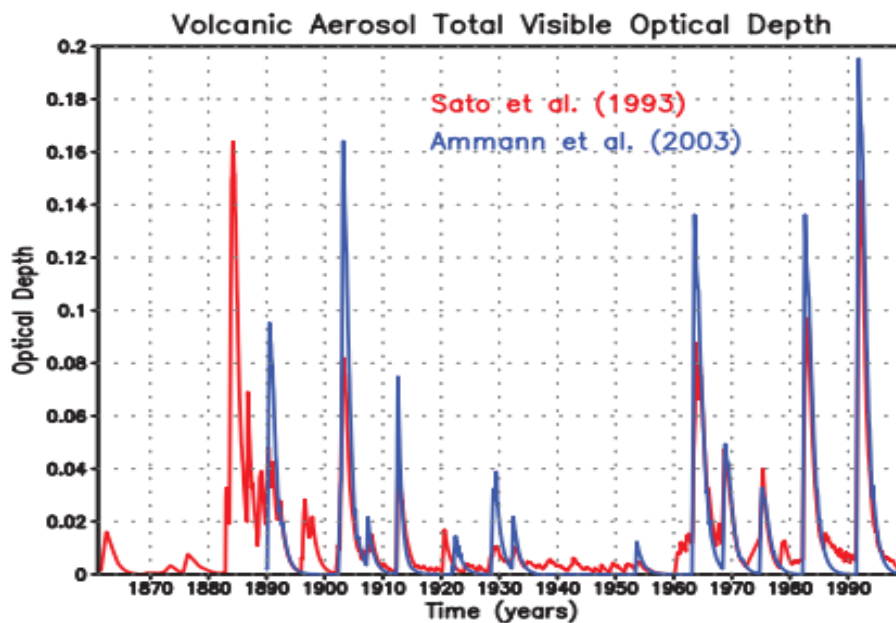


Figure 2.7: Visible optical depth estimations of stratospheric sulphate aerosols produced in the outcome of tense volcanic eruptions between 1860 and 2000.

2.4 Atmospheric Forcings

Precipitation can react to both changes to the forcing agent itself and in temperature. The dependence of the precipitation response on the nature of the forcing agent is next considered (O’Gorman et al., 2011). In addition, an increase in CO₂ concentrations leads to the decline in the net upwelling long wave radiation at TOA as well as increase in the net downwelling long wave radiation at the surface ($\Delta R_{TOA} > \Delta R_{SFC}$). The above procedure decreases net radiative cooling of the atmosphere (Ramanathan 1981; Mitchell et al. 1987; O’Gorman et al., 2011). Therefore, the atmosphere is heated and stabilised causing a decline in the precipitation rate.

On the other hand, precipitation responds to changes in temperature (ΔT) via various climate feedbacks that influence precipitation processes (2-3%K⁻¹) (Held and Soden, 2006; Lambert and Webb, 2008). For example, an increase in surface temperature causes stronger radiative cooling of the atmosphere which is evened out by stronger precipitation rate. The timescales of these two processes are different because of the small atmospheric heat capacity related to the ocean. For instance, in response to the increased amount of CO₂, the precipitation rate goes down first because of the direct atmospheric response but later increases linked with ΔT (Bala et al., 2009). The above precipitation responses are referred to as fast (ΔP_{fast}) and slow (ΔP_{slow}) responses respectively. The total change of precipitation is given by summing these two precipitation responses.

In order to test which constituents of RF are a good predictor for the fast and slow precipitation responses, forcings at the TOA and the surface are assumed to be bad predictors of ΔP_{fast} , while atmospheric forcing is supposedly a good predictor. The reason of this good correlation between the atmospheric forcing and the fast precipitation response can be explained from energetic grounds (e.g., Allen and Ingram, 2002). Any perturbation in atmospheric radiative cooling is balanced by changes in precipitation rate.

The computation of RFs at the atmosphere is accomplished using both forcings at the top of the atmosphere, which are evaluated by the spread-sheet and are described in section 2.3 whilst forcings at the surface are estimated using the following equation:

$$F_{SFC} = R \times F_{TOA} \quad (5)$$

where R is the ratio of instantaneous surface forcings over forcings at the TOA, is evaluated by Andrews et al., 2010 and its detailed description is given in the following section (2.5). The atmospheric forcing is described by the following equation:

$$F_{ATM} = F_{TOA} - F_{SFC} \quad (6)$$

$$\stackrel{5,6}{\Rightarrow} F_{ATM} = F_{TOA}(1 - R) \quad (7)$$

2.5 Evaluation of ratio R

Direct sulphates, cloud albedo, and changes in solar constant are driving climate through the scattering of solar radiation and thus the atmosphere is transparent to these RFs ($R=1$). On the other hand, black carbon (BC) aerosol powerfully absorbs solar radiation in the atmosphere, leading to the decrease in solar radiation amount which reaches the surface but also lessens reflected solar radiation released to space. Thus, BC aerosol has a negative instantaneous RF at the surface and a positive RF at the top of the atmosphere (e.g., Ramanathan et al., 2001a), as shown in Table 2 where $R=-1.5$. (Andrews et al., 2010)

Biomass burning aerosol both disseminates and absorbs solar radiation. A negative RF is generated both at the TOA and surface through scattering and a small positive atmospheric component is produced as a result of the absorption, hence $R>1$. Ozone (O₃) RF is more complex than the ones previously mentioned due to *“the competing effects in solar and thermal spectra, as well as the competing increases and decreases in concentration through the troposphere and stratosphere”* (Andrews et al., 2010). The net global-mean effect is a value of R close to 1. Finally, the RF of carbon dioxide and methane, is mostly absorbed in the atmosphere and $R<1$ (Andrews et al., 2010). A representation of R values for the RFs that are used in this project is given in Table 2.

Table 2: Representation of R values for different radiative forcings which are used in this project. R is dimensionless (Andrews et al. 2010).

Forcing Scenario	$R = \frac{F_{SRF}}{F_{TOA}}$
CO ₂	0.2
CH ₄	0.5
Cloud Albedo	1.0
Solar	0.8
O ₃	1.3
SO ₄	1.0
BB	1.9
BC	-1.5

2.6 Representation of atmospheric forcings

Referring to sections 2.4 and 2.5, the atmospheric forcing time series of greenhouse gases, aerosols, and natural processes are illustrated below in Figures 2.9, 2.10 and 2.11. The radiative forcing (RF) of all well-mixed greenhouse gases is positive because they increase the absorption of excess radiation in the atmosphere. This occurs through the molecular rotational and rotational-vibrational modes of infrared and near-infrared photons (Collins et al., 2006). Their RFs also increase with height throughout the troposphere; hence it is mainly absorbed in the atmosphere (Figure 2.9). The positive RF shows the strong absorption of radiative energy by the climate system (Collins et al., 2006).

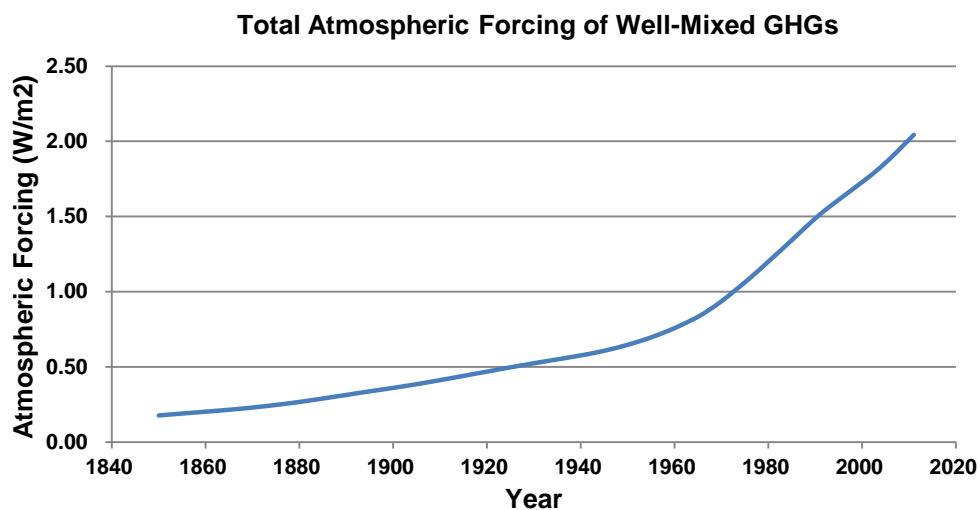


Figure 2.9: Illustration of the total atmospheric forcing time-series of all well-mixed greenhouse gases (GHGs).

On the other hand, aerosols were expected to have a negative atmospheric forcing, but as demonstrated in Figure 2.10, the atmospheric forcing of aerosols in this climate model gives a positive outcome which is enhanced throughout the years. This is generated because SO₄ and cloud albedo have an R close to unity, as referred above, due to the scattering of solar radiation. Therefore, their atmospheric forcing tends to zero according to Eq. 7. Biomass burning has a trivial RF at the TOA and thus is an insignificant atmospheric forcing. The major factor that causes this positive atmospheric forcing is black carbon (BC), as it strongly absorbs solar radiation in the atmosphere. It is also relevant that the aerosol forcing is more variable spatially; since this could lead to a rise in distinct regional responses.

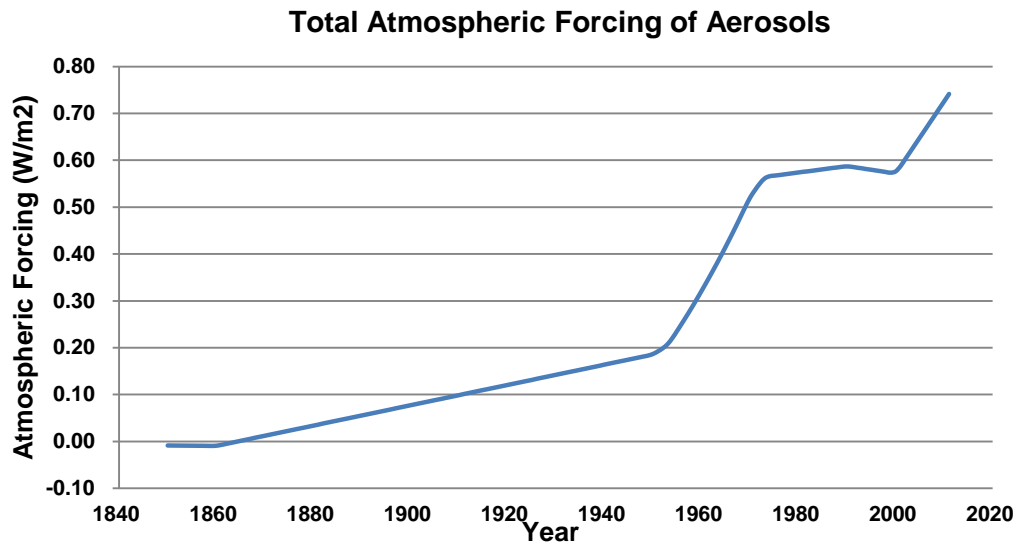


Figure 2.10: Illustration of the total atmospheric forcing time-series of aerosols.

In reference to Figure 2.11, the atmospheric forcing of natural processes follows a path strongly influenced by a well-established 11-year cycle of solar irradiance. In addition, volcanic eruptions can cause a short-lived negative forcing of two to three years through the temporary increase of sulphate aerosol in the stratosphere. Therefore, the value of R for volcanic eruptions equals to the value of sulphate aerosol ($R=1$). Thus, according to Eq. 7, the atmospheric forcing for volcanic eruptions tends to zero.

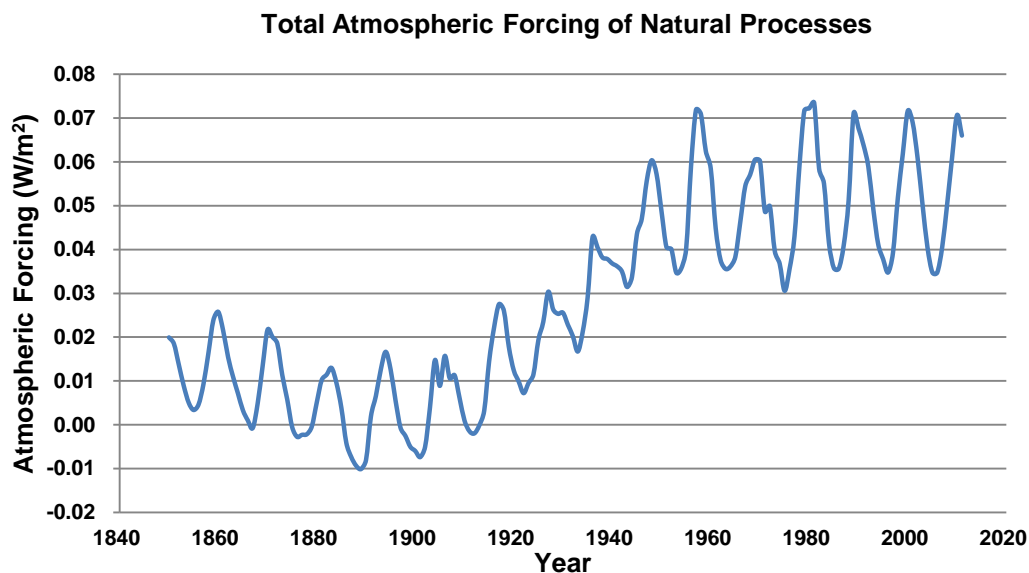


Figure 2.11: Illustration of the total atmospheric forcing time-series of natural processes.

2.7 Precipitation Rate

The linear dependence of precipitation on temperature, which has been illustrated By Hadley Centre Slab-Ocean Model version 3 (UKMO-HadSM3) (Andrews et al., 2009) represented in Figure 2.12, suggests the rearranging of Eq. 1, splitting the right hand side into a slow response to surface temperature anomalies ($\kappa\Delta T$) and a fast atmospheric response to RFs \mathbf{G} ,

$$L\Delta P = \kappa\Delta T_s + G \quad (8)$$

Where κ is a hydrological constant evaluated as 2-3 %K⁻¹ (Andrews et al., 2009) and ΔT_s represents the surface temperature anomalies which are already computed by the zero-dimensional model. \mathbf{G} is considered by Previdi (2010) as the direct atmospheric forcing. Therefore, Eq. 8 is rewritten as:

$$L\Delta P = \kappa\Delta T_s - \Delta F_{atm} \quad (9)$$

$$\stackrel{7,9}{\Rightarrow} L\Delta P = \kappa\Delta T_s - \Delta F_{TOA}(1 - R) \quad (10)$$

The hydrological sensitivity (κ), using the total precipitation response, varies significantly through the forcing agents, maintaining the result of recent climate studies that precipitation fluctuations strongly depend on forcing mechanisms. Andrews (2010) estimated the fast response of precipitation using fixed sea surface temperature. The fast response is essentially verified by the atmosphere-only integrations. In addition, the total change of precipitation is mainly the change of precipitation in the full atmosphere/mixed-layer integrations. Therefore, subtracting the fast atmospheric component from the total response, the slow response is evaluated. Andrews (2010) found that when only the slow components of the climate change were considered, the range of hydrological sensitivity is in good agreement across the forcing agents.

Figure 2.12 shows that the response of precipitation to a substantial increase of CO₂ is initially characterized by a reduction in precipitation rate followed by a linear enhancement with temperature. On the other hand, the precipitation responds to an increase of solar forcing following a similar path with the CO₂ but the initial decrease is smaller. In contrast to the the slopes of precipitation curves (solid and dashed lines in Figure 2.12) which are similar between the two forcings, the hydrological sensitivity differs significantly at equilibrium between the CO₂ and solar RFs (dotted lines in Figure 2.12)².

² It should be noted that when the hydrological sensitivity is determined in terms of RF at the TOA, it is quite similar between CO₂ and solar RFs (Lambert and Faull 2007).

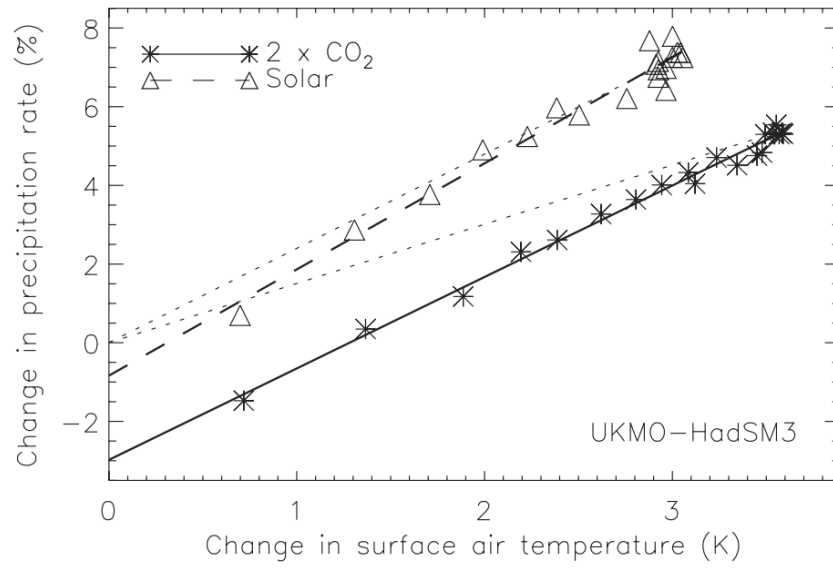


Figure 2.12: Change in annual global-mean precipitation rate (%) relative to annual-mean changes in temperature (ΔT) for the HadSM3 2xCO₂ and solar increase experiment. The precipitation adjustment before ΔT is larger for CO₂ experiment, but as ΔT enhances the precipitation response between these two forcing agents.

Chapter Three: Experiments and Results

3.1 Precipitation Response using GHGs radiative forcings

The initial experiment performed in this project focused on global-mean precipitation rate including only GHGs RFs. The slow component of precipitation, which is the component that scales with the change in surface temperature ($\kappa\Delta T$), is principally influenced by the RFs of well-mixed GHGs, a consequence that agrees with the new atmosphere-ocean climate modelling studies. A research shows that carbon dioxide is responsible for about 20% of the greenhouse effect (Lacis et al., 2010).

When the concentrations of well-mixed GHGs are rising (including CO_2 , the most significant well-mixed GHG), their RFs are positive due to the absorption of the outgoing infrared radiation in the atmosphere. The climate model evaluates a considerable increase in the RF of GHGs at the TOA (Figure 3.1), causing an enhancement in the global surface-air-temperature anomalies, ΔT_s , and thus in the slow component of climate change (Figure 3.1). The increase of surface temperature changes will increase the atmospheric temperature, for example if the moist adiabatic lapse rate (MALR) is conserved. A warmer atmosphere radiates energy away faster (stronger radiative cooling) and it becomes unstable more quickly. According to Andrews et al. (2010), radiative cooling of the atmosphere is balanced primarily by latent heating. Therefore, an increase of latent heat flux from the Earth's surface to the atmosphere is required, intensifying evaporation. Afterwards, the fast atmospheric component of precipitation is estimated (Eq.7), demonstrating an exponential increase in the atmospheric forcing time series (Figure 2.9 in Section 2.6). It is identified that the increase of atmospheric forcing tends to heat and stabilise the atmosphere and thus suppress the precipitation rate. On the other hand, the increase of ΔT_s , correlating with but lagging the increase of radiative cooling in the atmosphere, tends to enhance the precipitation rate.

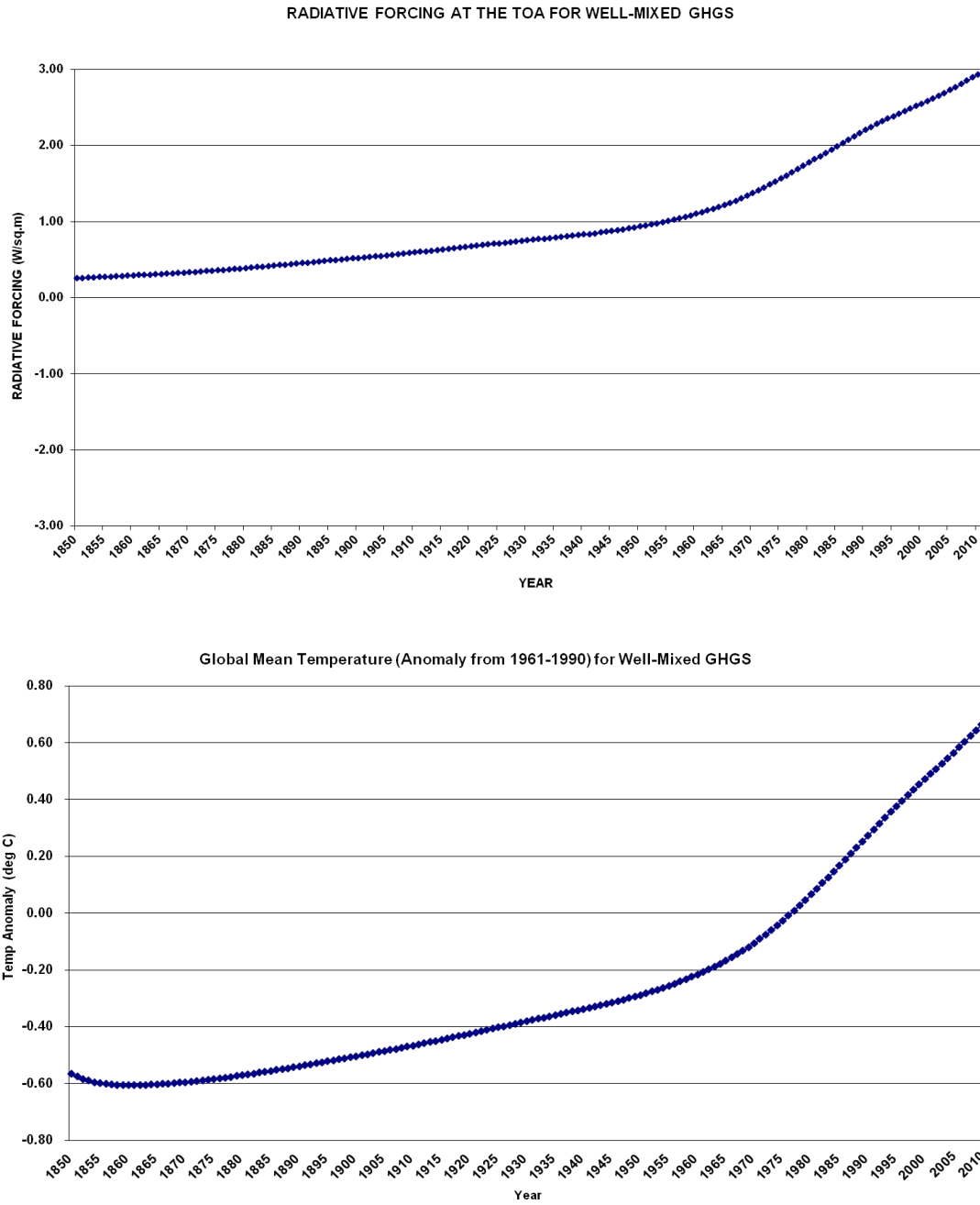


Figure 3.1: Illustration of total radiative forcing at the TOA and global mean temperature anomaly (relative to temperature anomaly from 1961-1990) for the well-mixed greenhouse gasses.

The climate model shows that the slow response to surface temperature anomalies increases faster than the quick atmospheric response to RF of well-mixed GHGs. This event tends to amplify the precipitation rate. The time series of the atmospheric forcing, surface temperature change, and global precipitation are illustrated in Figure 3.2.

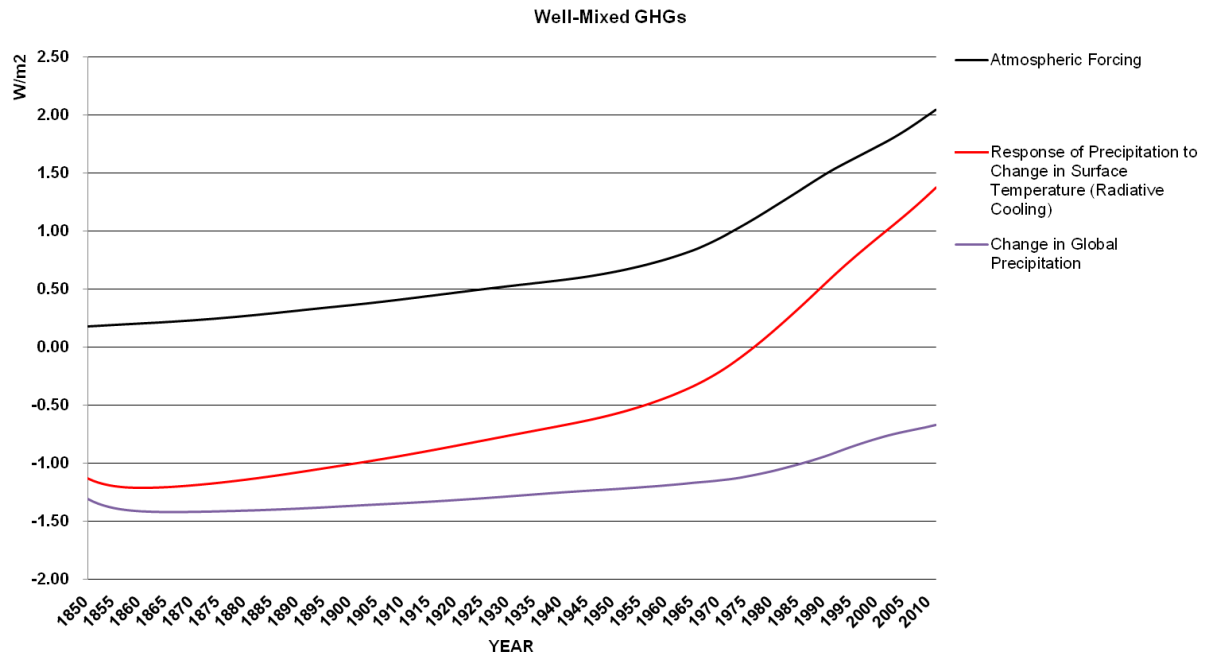


Figure 3.2: Time series of the atmospheric forcing, surface temperature anomaly and global precipitation time series for well- mixed greenhouse gases. The global mean precipitation increases as a consequence of the rapid increase of radiative cooling, increasing latent heat flux (from the Earth’s surface to the atmosphere) and convection.

The global mean surface temperature anomalies are not caused directly after the increase of GHGs concentrations; the full impact could take years or decades to be noticed. This lag is mostly because of the vast heat capacity of the oceans, which provides the climate with a thermal inertia that can cause surface warming or cooling gradually. This is the reason of the sudden increase of radiative cooling after 1950 in Figure 3.2.

3.2 Precipitation response using Aerosols radiative forcings

Aerosols also seem to have influenced significantly the global-mean precipitation primarily in two ways. They raise shortwave atmospheric heating, which suppress precipitation. Relying on the TOA radiative flux change, they can also heat or cool the surface and change the global-mean precipitation. The effects of absorbing aerosols vary with their height, but they diminish precipitation rate in most cases (Ming et al., 2010). The further shortwave (SW) absorption enhances atmospheric warming, decreasing latent heating. Aerosols are categorized into two groups, scattering and absorbing aerosols. Scattering aerosols, such as direct sulphate, have negative RFs at the TOA as they scatter incoming solar radiation. On the other hand, the RFs of absorbing aerosols,

such as black carbon, are positive due to the strong absorption of solar radiation in the atmosphere (Andrews et al., 2010).

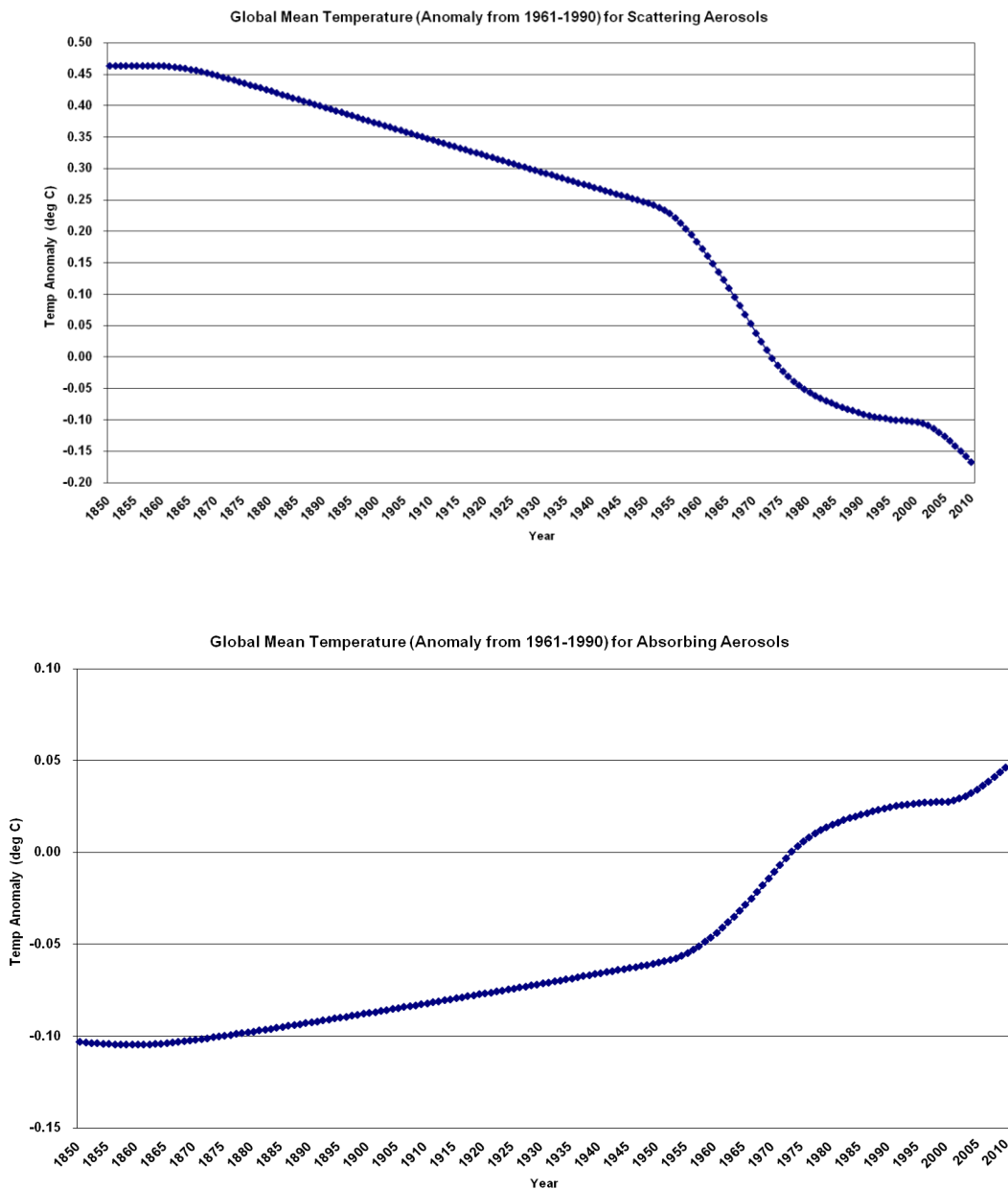


Figure 3.3: Illustration of global mean temperature anomaly (relative to temperature anomaly from 1961-1990) for both scattering and absorbing aerosols.

The climate model evaluates a pronounced increased magnitude in the RF of absorbing aerosols at the TOA. This leads to the enhancement of surface-air-temperature anomalies, ΔT_s , and thus in the slow component of precipitation. On the other hand, the increasingly negative RF of scattering aerosols, including cloud albedo indirect effects, triggers a decreasing temperature anomaly trend (Figure 3.3).

It should be mentioned that the aerosol forcing is highly uncertain. These uncertainties can be caused by the poor knowledge about the amount and the distribution of anthropogenic aerosols (especially before industrial era). Models also cannot represent precisely convection processes, updraft velocities and convection-cloud interactions leading to high uncertainties for cloud albedo effect (Lohmann and Feichter, 2005). Even if the biases in the model-generated clouds were ignored, the differences in the chemical composition of aerosols cause difficulties in the quantification of uncertainties.

The insignificant increase of surface temperature anomalies for absorbing aerosols will increase the atmospheric temperature, attempting to conserve moist adiabatic. The warmer atmosphere will enhance radiative cooling and precipitation rate. The fast component of precipitation presents a significant increase (Figure 2.10 in Section 2.6), tending to suppress the precipitation rate.

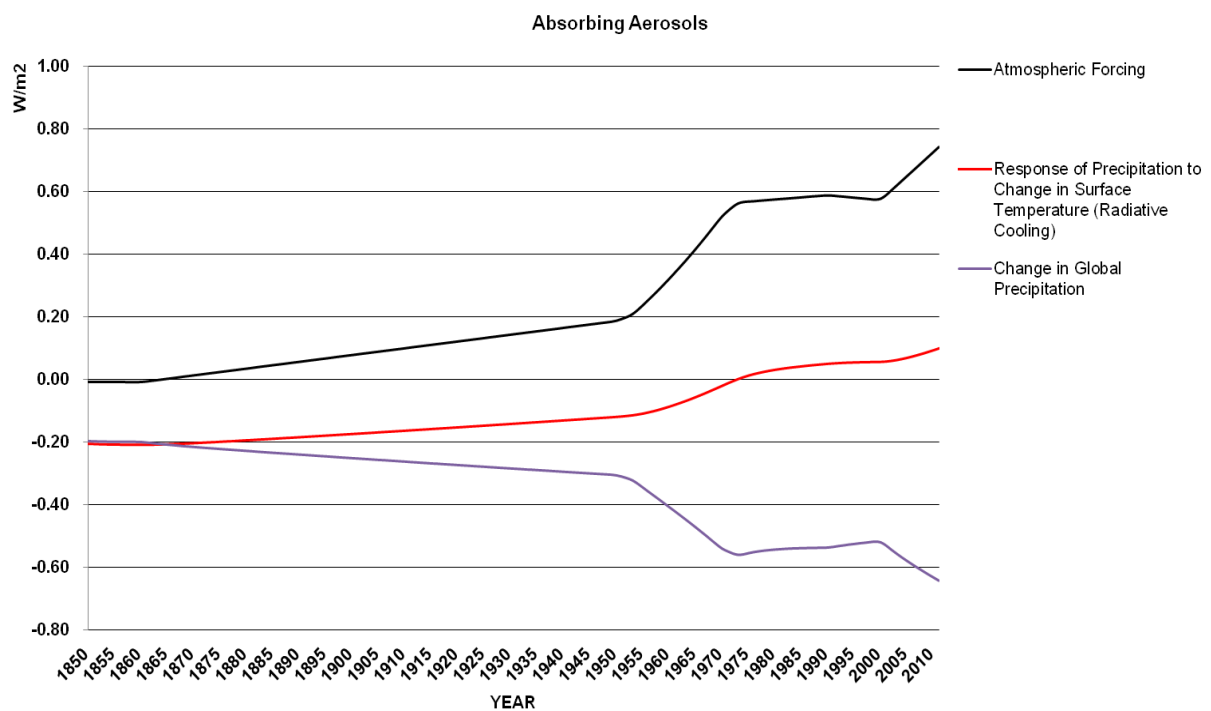


Figure 3.4: Time series of the atmospheric forcing, change in surface temperature, and global precipitation for absorbing aerosols. The global mean precipitation decreases because of the distinct increase of atmospheric forcing, increasing atmospheric stability and reducing convection (Dong et al., 2009).

The simple climate model shows a decrease of precipitation rate as the quick atmospheric component of precipitation increases faster than the slow response to global surface temperature anomalies. This is partly due to the absorption of incoming solar radiation by the absorbing aerosols in the atmosphere and the insignificant warming of surface temperature which is not sufficient to cause a strong radiative cooling (Figure 3.4). Most of modelling studies agree that increased absorbing aerosols RFs suppress precipitation rate. There are also some studies which disagree with this statement (Ming et al., 2010).

Dong et al., 2009 investigate the transient adjustment processes of the surface and troposphere where RF agents are turned on. They focus on the doubling of CO₂ concentrations showing that the warming of the surface is spreading upwards to the troposphere. According to the vertical warming over land, there is a rapid warming and moistening in the troposphere over the sea which is led by the response of surface to SST change. This warming is associated with a reduction in precipitation. They also mentioned that the processes which are described are analogous to RF by absorbing aerosols such as BC.

On the other hand, the decreasing temperature anomaly trend for scattering aerosols will decrease the atmospheric temperature. A cooler atmosphere radiates energy away slower (weaker radiative cooling) and is more stable. In reference to the weaker radiative cooling, the latent heating will also decrease. According to Andrews et al. (2010), the atmosphere is largely transparent to the RFs of scattering aerosols ($R=1$). Consequently, the atmospheric forcing given by Eq.7 tends to zero, leading to the reduction of precipitation rate.

The total RF at the TOA including both absorbing and scattering aerosols is negative (Figure 2.4 in Sub-section 2.3.3), leading to a decrease in the magnitude of global surface-air-temperature anomalies and consequently in the slow component of climate change (Figure 3.5). The climate model shows that the aerosols are dominated by the slow response to surface temperature anomalies, suppressing precipitation rate. The time series of the atmospheric forcing, change in surface temperature, and global precipitation are represented in Figure 3.5.

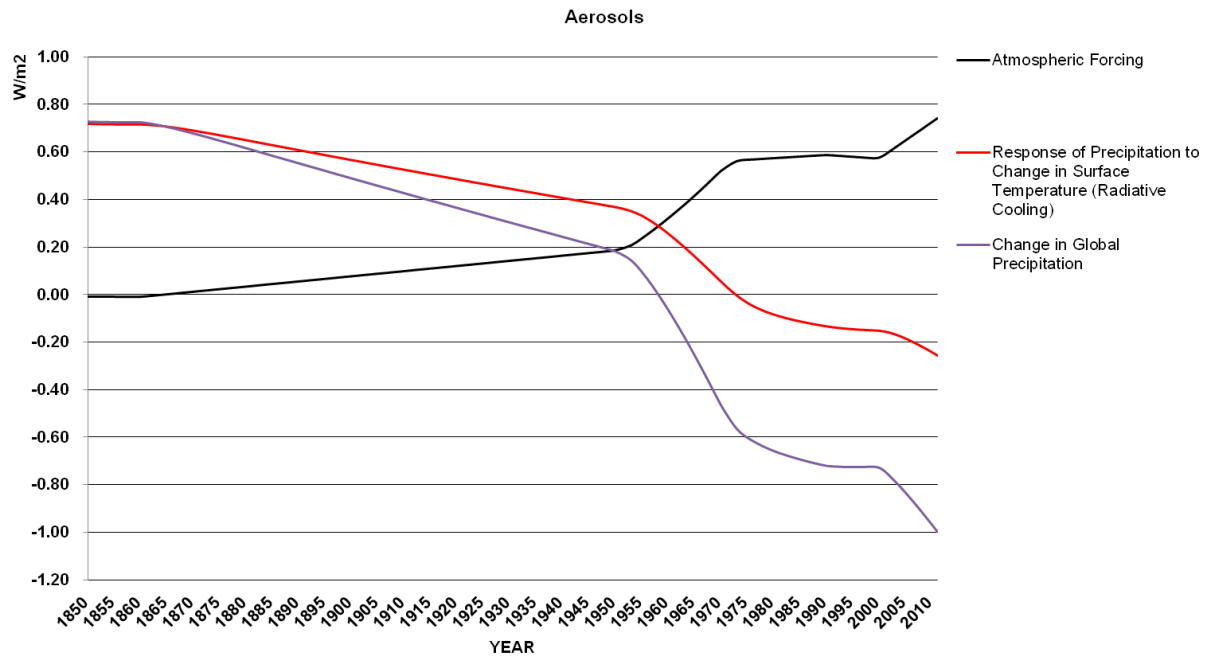


Figure 3.5: Time series of the atmospheric forcing, change in surface temperature, and global precipitation for all aerosols. The global mean-precipitation decreases due to the pronounced decrease of radiative cooling which leads to the reduction of latent heat flux and convection.

3.3 Precipitation Response using natural radiative forcings

Natural forcings are caused by solar changes and unpredictable volcanic eruptions. Solar output has increased slightly in the industrial era, determining a small positive RF. This is correspondent to the 11-year solar cycle; when the sun experiences a period of augmented magnetic and sunspot activity termed the solar maximum, followed by a quiet period called the solar minimum (NASA, 2003). Up to the 1970s, an increase of solar radiation has been observed. This enhancement is estimated to be nearly 0.05% per decade (NASA, 2003). Richard Wilson mentioned that “this trend is important because, if sustained over many decades, it could cause significant climate change” (NASA, 2003). On the other hand, volcanic eruptions can cause a short-lived negative RF at the TOA due to the increase of sulphate aerosols in the stratosphere. The RF of both solar irradiance and volcanic eruptions at the TOA are illustrated in Figure 3.6.

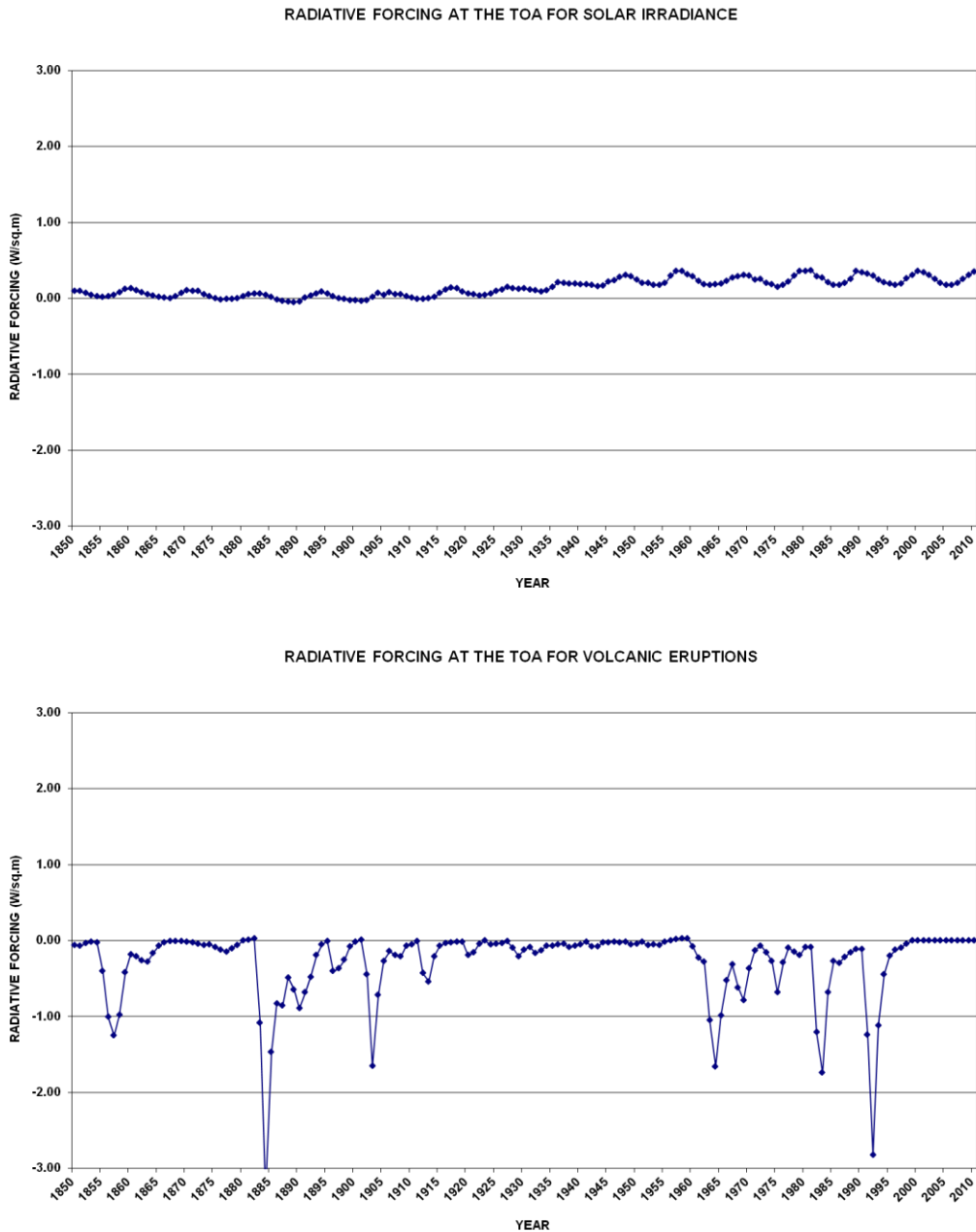


Figure 3.6: Illustration of total radiative forcing at the top of the atmosphere for a) solar irradiance and b) volcanic eruptions. The 11-year cycle of solar radiation is pronounced in the trend-line of solar irradiance. The biggest volcanic eruptions of Krakatoa (1883) and Mt. Pinatubo (1991) are indicated in the trend line for volcanic eruptions.

The global mean-temperature anomalies for both solar irradiance and volcanic eruptions (Figure 3.7) show that the temperature anomalies follow the trend of their RFs at the top of the atmosphere, demonstrating the 11-year solar cycle, the gradual increase of solar irradiance the last decades (NASA, 2003), and the sudden, pronounced cooling of the air-surface temperature by the volcanic eruptions.

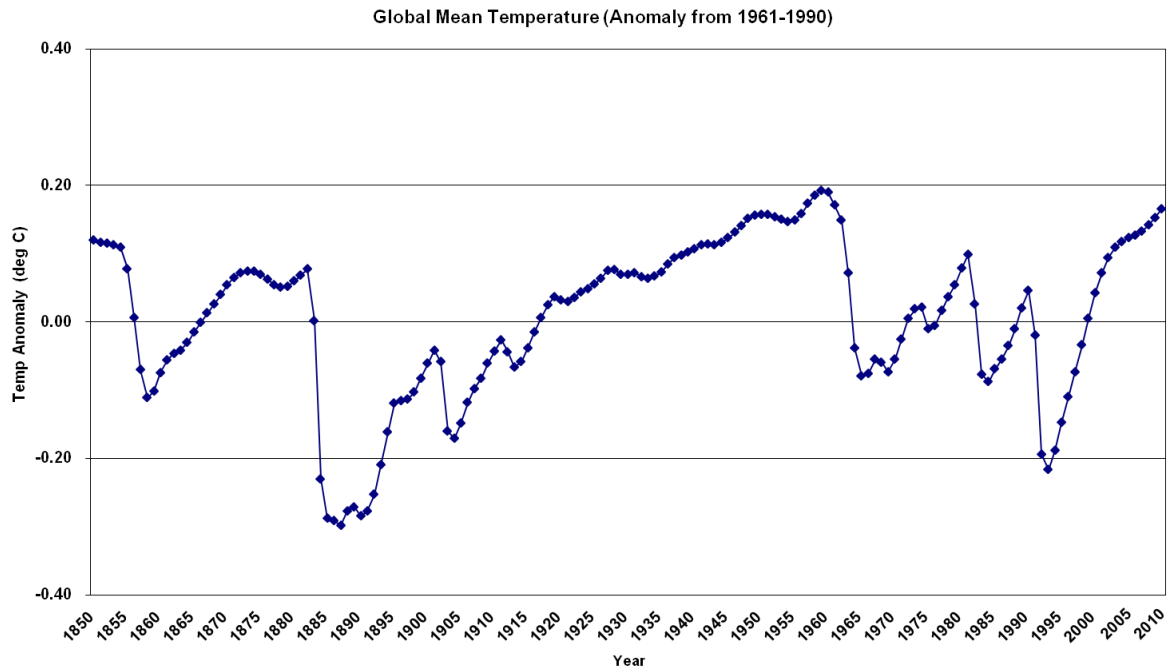


Figure 3.7: Illustration of global mean temperature anomaly (relative to temperature anomaly from 1961-1990) for the natural processes. The short-time minima are caused by volcanic sulphates and they agree with the literature as it can be observed that their effect lasts 2-3 years. The 11-years solar cycle is distinctly noticed from 1915 to 1960, when non-strong eruptions were observed according to the simple, zero-dimensional climate model.

The negative RF of volcanic sulphates due to the scattering of incoming solar radiation causes significant global surface-air temperature anomalies, decreasing the component of precipitation. The decrease of surface temperature will decrease the atmospheric temperature, reducing the precipitation rate. The trivial positive RF of the solar irradiance does not present extensive changes except the slight increase from 1900-1950, as it can be noticed in Figure 3.6.

Afterwards, the atmospheric forcings of both natural processes are estimated (Eq.7), demonstrating the 11-year solar cycle without the volcanic perturbations (Figure 2.11 in Section 2.6). As mentioned above, the atmosphere is largely transparent ($R=1$) for climate change mechanisms such as volcanic sulphates, leading to an atmospheric forcing which tends to zero. However, the value of ratio R for solar irradiance is evaluated to be 0.8, as an amount of solar irradiance is absorbed by the atmospheric water vapour and ozone. The climate model shows that the global mean-precipitation changes are dominated by the slow response to surface temperature anomalies, as it is established by Figure 3.8.

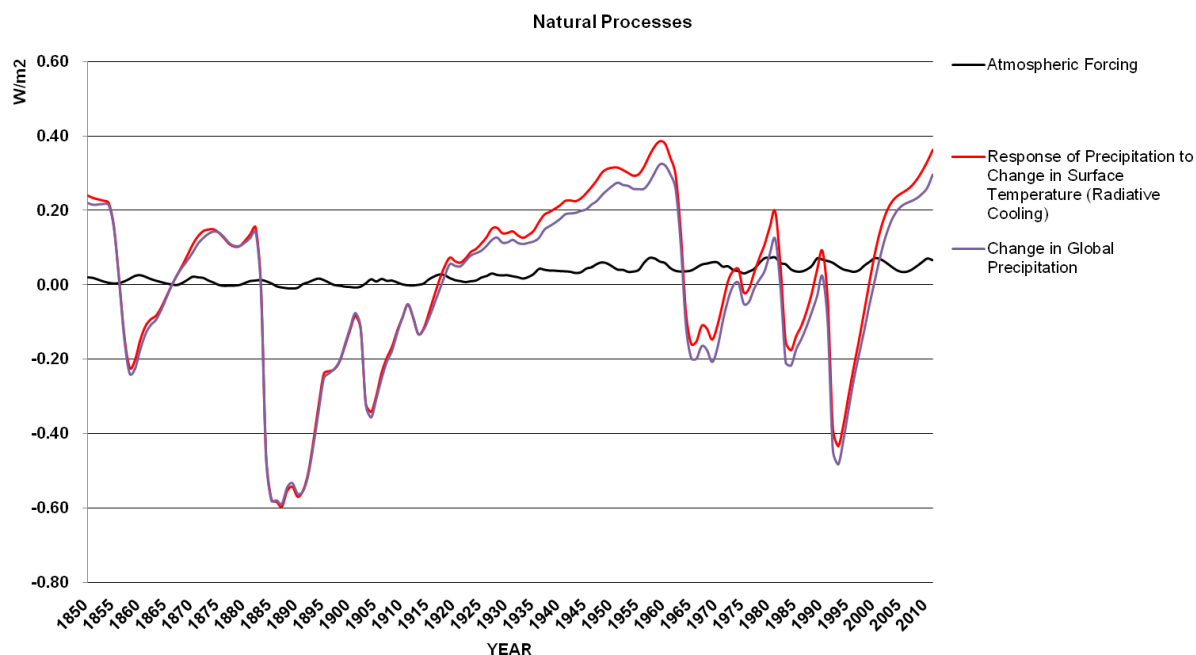


Figure 3.8: Time series of the atmospheric forcing, surface temperature anomaly, and global precipitation for natural processes. The global mean-precipitation considerably varies according to the radiative cooling which leads to short-term enhancements or reductions of latent heat flux and convection. The atmospheric forcing is related only to the solar irradiance, following the 11-year solar cycle, but it does not play an important role in the determination of annual global mean-precipitation rate.

3.4 Precipitation response using all radiative forcings

The RFs which are included in the simple global mean, zero-dimensional, climate model were categorized into three categories, greenhouse gases, aerosols, and natural processes. In this section, all the RFs are combined and a detailed discussion about the results and the major forcings that determine global mean precipitation, surface temperature anomalies and atmospheric forcing is given. The total RF at the TOA, including all RF terms listed in the simple climate model, is illustrated in the following graph (Figure 3.9).

The negative RF of volcanic aerosols due to the short-lived increase of sulphate in the stratosphere plays an important role in the evaluation of total RF at the TOA (red line in Figure 3.9). It can be observed that before 1915, the amount of greenhouse gases, according to the climate model, was not crucial, as it did not balance significantly the negative RF of strong volcanic eruptions. For example Krakatoa (1883) initially had a negative RF of -3.3Wm^{-2} , but including greenhouse gases and aerosols (both absorbing and scattering aerosols) the RF is reduced to -3Wm^{-2} . Since 1915, the RF of volcanic eruptions has demonstrated an apparent decrease because it is balanced by the positive RF

of well-mixed greenhouse gases and absorbing aerosols. For instance, Mt. Pinatubo (1991) caused only -1Wm^{-2} RF due to the pronounced enhancement of the positive well-mixed GHGs and black carbon RFs at the TOA.

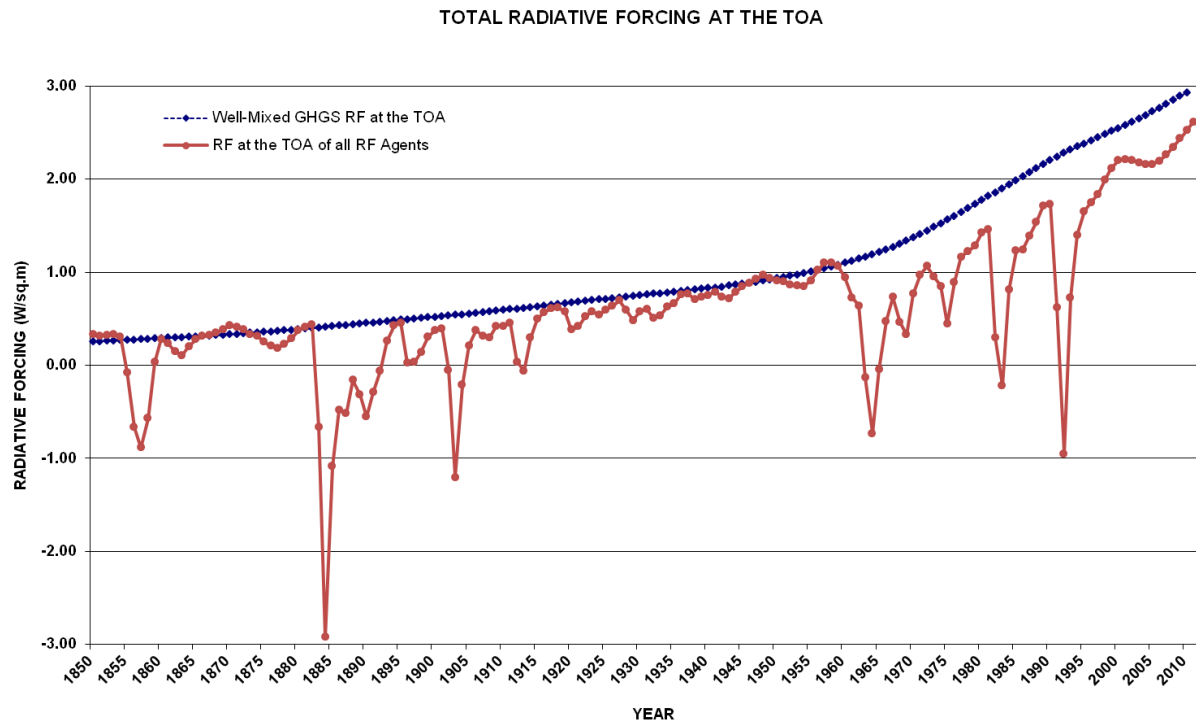


Figure 3.9: Illustration of total radiative forcing at the top of the atmosphere, including all radiative forcing terms introduced by the climate model (red line). The most significant RF terms that can be noticed are the volcanic eruptions, solar irradiance, greenhouse gases, and absorbing aerosols. The blue line represents the RF at the TOA running only for the well-mixed greenhouse gases.

In addition to the crucial changes by the volcanic eruptions, scattering aerosols (negative RF) attempt to balance absorbing aerosols and GHGs RF. According to literature (IPCC, 2007: Climate Change 2007-The Physical Science Basis) and climate model, the total RF of aerosols, including both scattering and absorbing aerosols, is negative but the large RF of well-mixed GHGs cancels it. Therefore, if the scattering aerosols were not considered, the peak-values in Figure 3.9 would be larger (tend to 4W/m^2) and the dip value would be smaller. RF of solar irradiance also affects the path of total RF at the TOA. The periodic motion of the 11-year solar cycle can be monitored by the red line in Figure 3.9, mainly between 1915 and 1960. Turning off the RF of solar irradiance, this period was smoother without peaks and troughs. In general, it is observed that the strongest RF terms at the TOA are the GHGs and the volcanic eruptions.

The path of global mean temperature anomaly including all RF terms (Figure 3.10), relative to 1961-1990, follows the increase in temperature anomaly for GHGs but there were some periods of strong,

short-lived (on a scale of 2-3 years) decreasing temperature anomaly trends. These decreases are related to the volcanic eruptions. The biggest drop of temperature anomaly was observed in 1883 when it reduced from -0.20°C to -0.65°C due to the strong volcanic eruption of Krakatoa. It is noticed that the decreases of temperature anomaly due to the volcanic eruptions are less crucial during the recent decades. The reason for this effect is the enhancement of the positive RF of GHGs, as they are long-lived and well-mixed in the atmosphere. This causes a rapid increase in surface-air temperature which is not temporary, like the decrease of temperature by the short-lived volcanic sulphates. For the past years (e.g. 1883), the simple climate model evaluates slightly small values for the RF of well-mixed GHGs and this responds to the lag of the climate system to balance the perturbations by the volcanic eruptions.

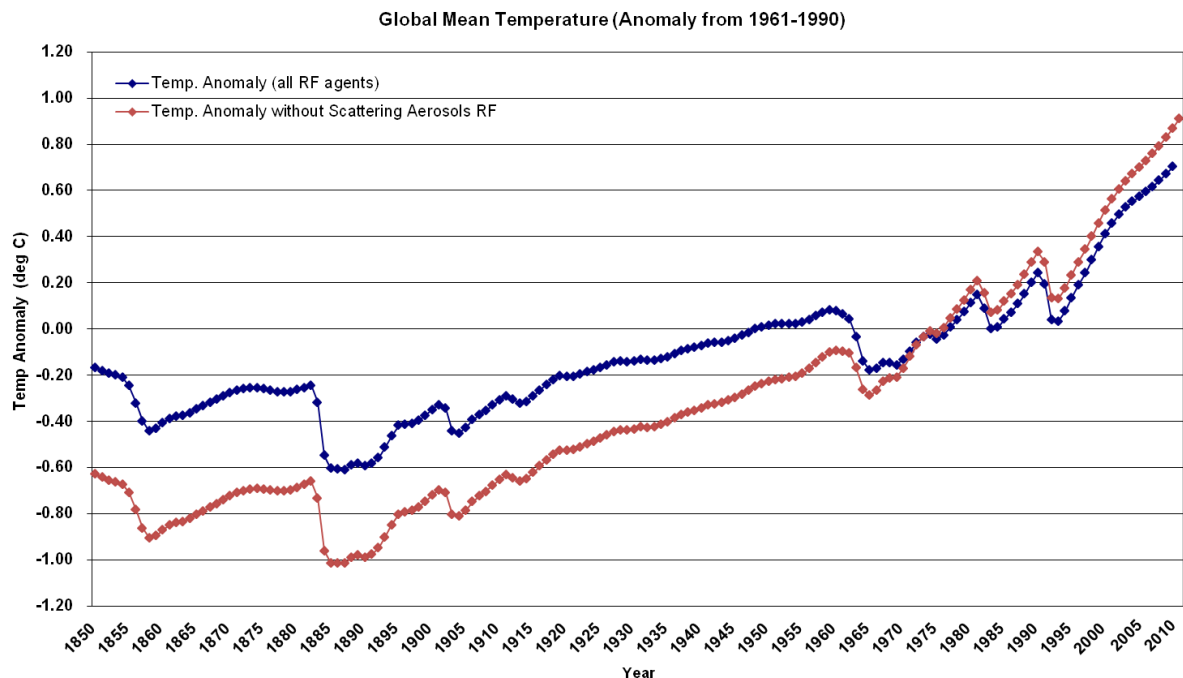


Figure 3.10: Illustration of global mean temperature anomaly including all RF terms. The short-time minima are caused by volcanic sulphates. They agree with the literature (e.g. Ammann et al., 2003) as it can be observed that their effect lasts 2-3 years. The 11-years solar cycle is discernible from 1915 to 1960, when no strong eruptions were observed. The increase of temperature anomaly in the last decades is caused by the GHGs and it would be more rapid if the scattering aerosols were not taken into account. The red line represents the global mean temperature anomaly without including the scattering aerosols RF.

In addition to well-mixed GHGs and volcanic eruptions, aerosols play a significant role in the evolution of global mean temperature. Scattering aerosols which have a negative RF tend to balance the temperature perturbations caused by absorbing aerosols and GHGs. Turning off the RFs of scattering aerosols, the magnitude of global mean temperature anomalies is increased (red line in Figure 3.10). RF of solar irradiance also influences the trend-line of global mean temperature

anomaly similarly to the total RF at the TOA. The 11-year solar cycle can also just be noticed in Figure 3.10 from 1915 to 1960.

The anthropogenic and natural scattering aerosols which scatter the incoming solar radiation reduce the precipitation rate (-2Wm^{-2} is the maximum decrease found by the climate model and is illustrated in Figure 3.11). On the other hand, absorbing aerosols and GHGs, which absorb incoming solar radiation and trap the outgoing infrared radiation, enhance the precipitation rate.

The total atmospheric forcing is essentially defined by the GHGs, solar irradiance and absorbing aerosols, as the atmosphere is transparent to scattering aerosols and volcanic eruptions. The path of total atmospheric forcing which is represented by the black line in figure 3.11 shows a linear increase in the last four decades. This is due to the strong effect of GHGs and the recovery from volcanic cooling but also a continuous periodic motion signifies the 11-year solar cycle.

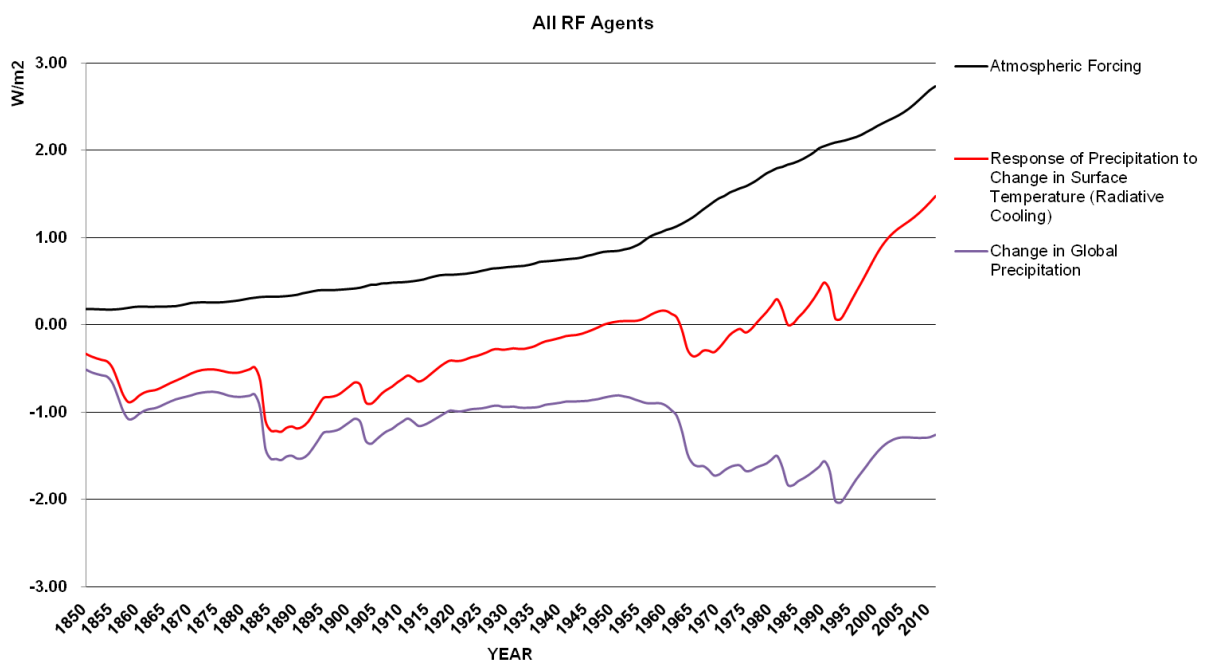


Figure 3.11: Time series of the atmospheric forcing, changes in surface temperature and global precipitation for all RF terms. The global mean-precipitation generally reduces as quick atmospheric response to RFs increases more rapidly than the slow response to surface T anomalies. Further temporary reductions (about 2 to 3 years) of global mean-precipitation are related to the occasional volcanic eruptions.

The climate model shows that the fast atmospheric component of precipitation is increasing faster than the slow response to surface temperature anomalies. Further temporary decreases in

precipitation are observed occasionally, related to the volcanic eruptions. The time series of the atmospheric forcing, surface temperature anomalies and global precipitation are represented in Figure 3.11.

3.5 Precipitation response changing R value

Each RF term has a different value for the ratio R, as mentioned in section 2.5. Black carbon has the most significant value ($R_{BC}=-1.5$), as it absorbs solar radiation in the atmosphere, reducing the amount of solar radiation which reaches the Earth's surface but also reduces outgoing infrared radiation. Therefore, the F_{SRF} is negative while F_{TOA} is positive, explaining the negative value of ratio R which is evaluated by Andrews et al., 2010. Changing the value of ratio R for BC to -2.5, an increase in atmospheric forcing is observed (black line in Figure 3.12). It is identified that the increase of atmospheric forcing tends to heat and stabilise the atmosphere and thus suppress the precipitation rate (purple line in Figure 3.12).

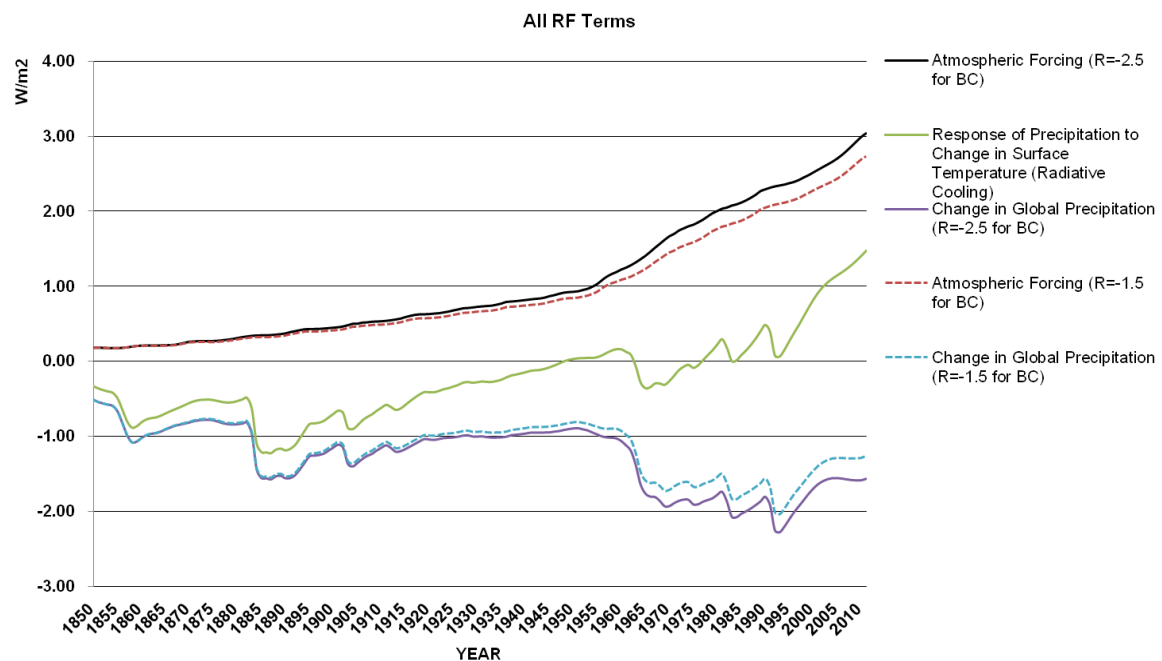


Figure 3.12: Time series of the atmospheric forcing, surface temperature changes, and global precipitation for all RF terms, using $R=-2.5$ for black carbon instead of $R=-1.5$. The global mean-precipitation generally reduces as the atmospheric forcing (fast component of climate change) increases more rapidly than the radiative cooling of the atmosphere (slow component of climate change). Further temporary diminutions (about 2 to 3 years) of global mean-precipitation are related to the occasional volcanic eruptions. The dashed lines represent the results using the value of R_{BC} evaluated by Andrews et al., 2010.

This can mathematically be explained using Eq.7. By negatively increasing further the value of the ratio R ($R_{BC} < -1.5$), the RF of black carbon at the TOA decreases according to Eq.5. This considerable decrease diminishes the magnitude of global surface-air-temperature, ΔT_s . The decrease of ΔT_s , correlating with the decrease of radiative cooling in the atmosphere, is likely to suppress the precipitation rate, as the atmosphere warms up and becomes stable.

The result of this experiment does not present a realistic case, as the RF at the TOA is not able to be changed due to the values being fixed, as mentioned in section 2.3. However, the fast atmospheric component of precipitation increases faster than the slow response to surface temperature anomalies. This event suppresses the precipitation rate according to eq.8. The additional, temporary oscillations in precipitation rate are caused by the volcanic eruptions. For example, using $R=-2.5$ the value of global precipitation change equals to -2.3 Wm^{-2} (-0.08 mm/day) on 1991 during the eruption of Mount Pinatubo, while using $R=-1.5$ (evaluated by Andrews et al. 2010) the value of precipitation change on 1991 is -2 W/m^2 (-0.06 mm/day).

3.6 Precipitation response changing feedback parameter

In reference to Section 2.2, if Q is the net radiation absorbed by climate system measured at the TOA, in a global and annual mean sense for a system in equilibrium, it equals to zero:

$$Q = ASR - OLR = 0$$

where ASR is the absorbed solar radiation and OLR is the outgoing long wave radiation. When the climate system is in equilibrium the ASR equals to the OLR. Therefore, the increased feedback parameter tends to balance the energy budget of the atmosphere and to diminish the changes of global mean-precipitation rate, while the reduced feedback parameter tends to cause further perturbation to the energy budget of the atmosphere, leading to the enhancement of global mean precipitation rate.

This can also be explained physically. The increase of feedback parameter to 3.3 Wm^{-2} leads to the reduction of global surface-air-temperature anomalies (ΔT_s) (red line in Figure 3.13). Therefore, it is identified that the decrease of ΔT_s , correlating with the decrease of radiative cooling in the atmosphere, tends to suppress changes in the global mean precipitation rate (Figure 3.14). On the other hand, a decrease of feedback parameter to 0.8 Wm^{-2} leads to an increase of global surface temperature anomalies (black line in Figure 3.13). This enhancement tends to increase the global

mean precipitation rate (Figure 3.14). The atmospheric forcing demonstrates the same path as none of the terms will be altered.

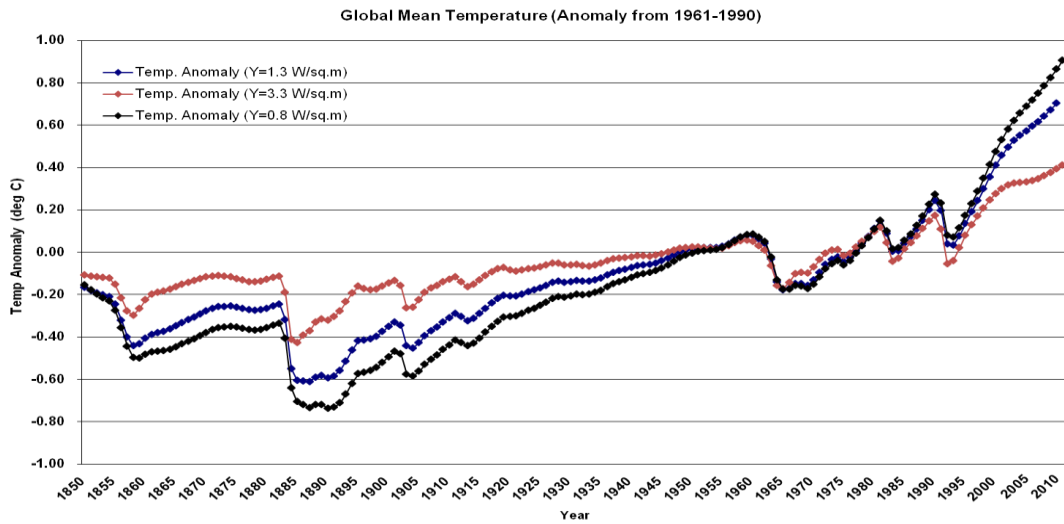


Figure 3.13: Comparison of time series of global mean temperature anomaly (relative to temperature anomaly from 1961-1990) including all RF terms with three different feedback parameter, $Y=3.3 \text{ Wm}^{-2}$ (red line), $Y=1.3 \text{ Wm}^{-2}$ (blue line) and $Y=0.8 \text{ Wm}^{-2}$ (black line).

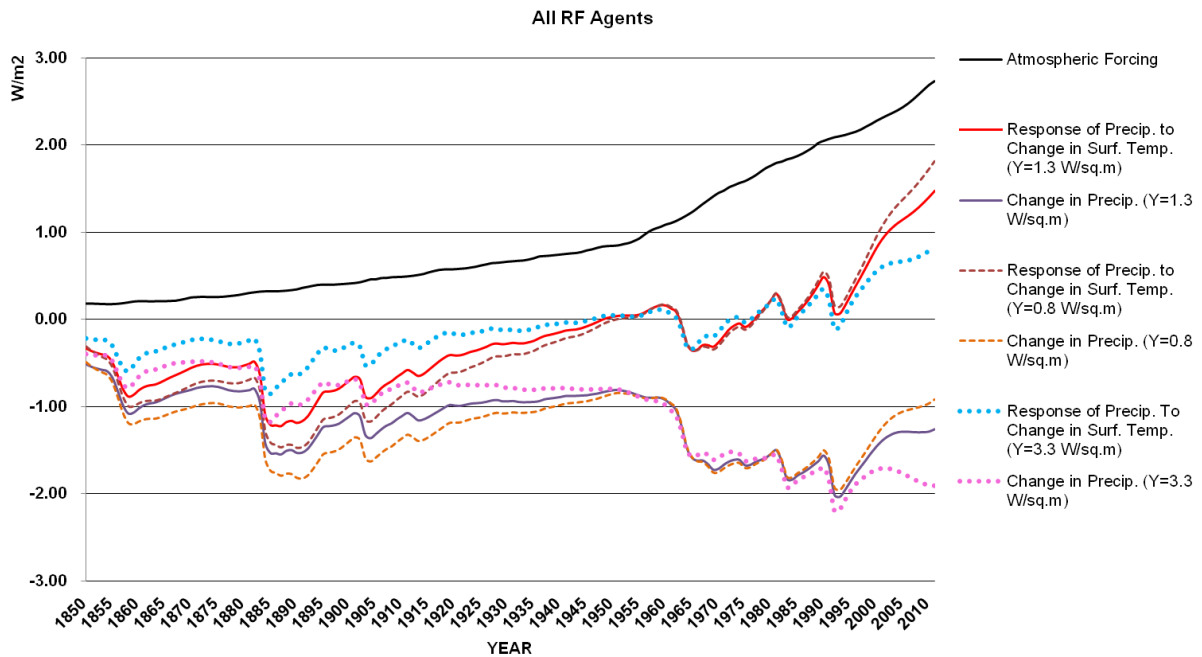


Figure 3.14: Time series of the atmospheric forcing, surface temperature anomaly, and global precipitation for all RF terms using three different feedback parameters, $Y=3.3 \text{ W/m}^2$, $Y=1.3 \text{ Wm}^{-2}$ and $Y=0.8 \text{ Wm}^{-2}$. The global mean-precipitation rate generally reduces as the feedback parameter increases and enhances when the feedback parameter decreases. Further temporary diminutions (about 2 to 3 years) of global mean-precipitation are related to the occasional volcanic eruptions.

Chapter Four: Comparison with Complex models and Observations

4.1 Observations

Observations for the energetic constraint on global precipitation are limited. Long-term observations of precipitation of approximately 50 years or more are narrowed to the land regions of northern hemisphere (Min et al. 2011), whereas ocean approximations are only obtainable by infrared (1979-1987) and microwave radiances (1987-present) (Huffman et al. 2009) including considerable uncertainties (Alder et al. 2001). Re-examination of surface temperature and pressure data can also be used to reconstruct past precipitation rates (Arkin et al. 2010); however, limitations are caused by the homogeneity between used input data and physical interactions.

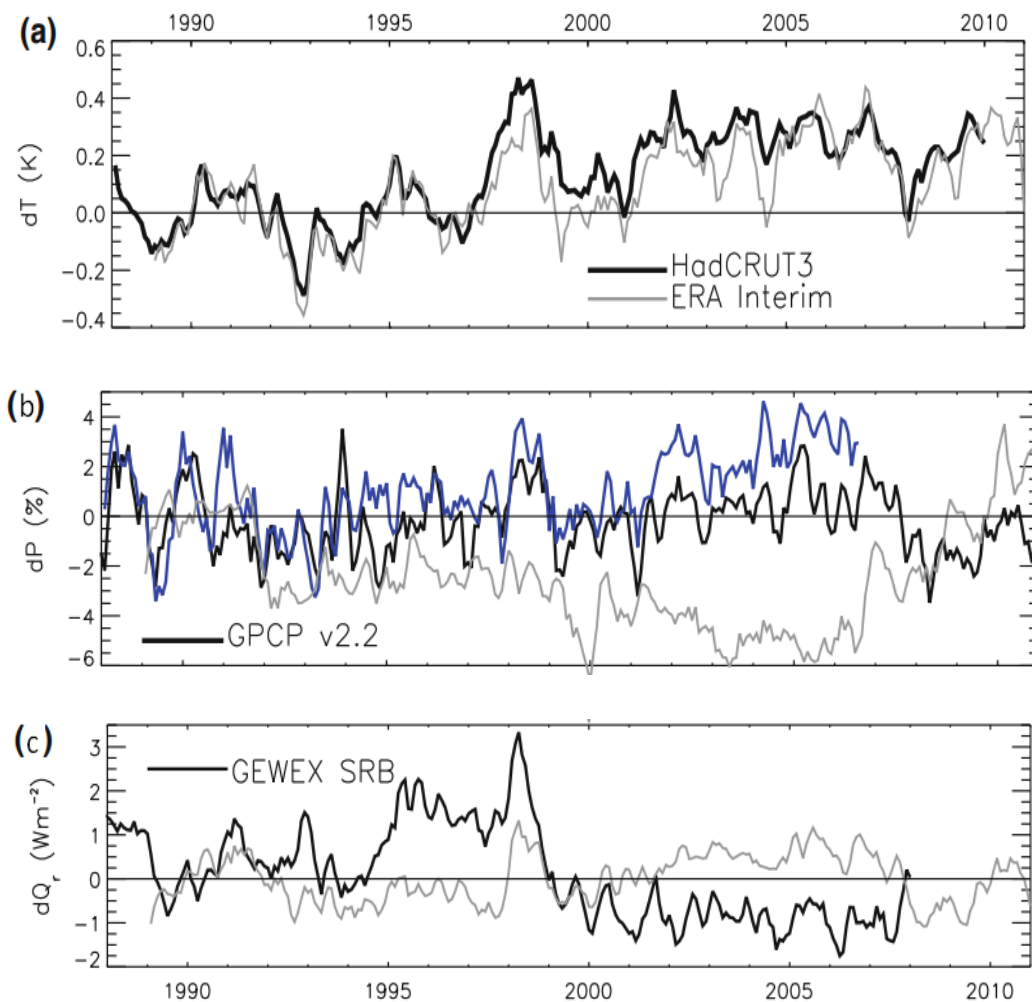


Figure 4.1: Time series of global mean anomalies in a) surface-air temperature, b) precipitation and c) total net radiative cooling of the atmosphere. (O’Gorman et al. 2011)

Historical estimations of Earth's radiative energy balance are more restricted than the observations of precipitation, as the satellite data have been provided since 1985 (Loeb et al. 2009) but with significant calibration (Trenberth 2002). In addition, surface measurements are narrowed to solar radiometers since the 1950s (Wild 1999). Consequently, the need of reanalyses data sets associated with complex modelling is essential to estimate the latest atmospheric radiative balance perturbations (Zhang et al. 2004).

Figure 4.1 illustrates the time series of global-mean surface temperature, changes in precipitation rate, and total net radiative cooling of the atmosphere. From 1990 to 2010, the global mean surface temperature varied by up to 0.8 K, principally relating to ENSO. However, the observed surface cooling in 1992 was triggered by the volcanic eruption of Mount Pinatubo in 1991.

4.1.1 Global-mean Precipitation Changes

Global Precipitation Climatology Project (GPCP v2.2) has been used to observe changes in global-mean precipitation (Huffman et al. 2009), combining infrared and microwave radiances over ice-free oceans since 1988 as well as rain-gauge measurements over the land (O’Gorman et al. 2011). The result in Figure 4.1b can be compared to the simulated precipitation rate from ERA Interim which demonstrates a downward trend up to 2005 (John et al. 2009) and a pronounced enhancement from 2006 to 2010 (Dee et al. 2011). As the hydrological cycle in reanalyses is not easily controlled in a global scale, decadal changes in global mean precipitation rate are not realistic (O’Gorman et al., 2010).

Using the data for surface temperature estimated by HadCRUT3 and global precipitation from GPCP over the period 1989-2008, a hydrological sensitivity is evaluated to be approximately 3.4 %K⁻¹ from 1989 to 2008, similar to values assessed by Adler et al. (2008) and Andrews et al. (2010). However, it is smaller than that evaluated by Wentz et al. 2007 (7%K⁻¹) for a shorter time period (Adler et al. 2008). The estimation introduced by Wentz et al. 2007 is established using linear trends in temperature and precipitation that present considerable uncertainties provided the short length of the climate record and the impact of ENSO and volcanic eruptions (Lambert et al. 2008). The larger precipitation response from 1987 to 2006 is possibly associated with a significant strengthening of the Walker and Hadley circulation since 1979 (Li et al. 2011). Arkin et al.(2010) generated 20th century precipitation rates based on surface temperature, pressure data, and observations over the

land suggesting a hydrological sensitivity of 2.5 %K-1 which agrees with Andrews et al. (2010) who suggested a value of 2-3 %K-1 (O’Gorman et al. 2011).

4.1.2 Net radiative cooling

Global mean precipitation changes are governed by radiative cooling of the atmosphere. The estimations of radiative cooling by NASA Global Energy and Water Cycle Experiment Surface Radiation Budget project do not fit each other very well (Stackhouse et al., 2011). This project employs information about clouds and radiation given by satellite profiles from reanalyses and the ERA Interim project (Zhang et al., 2004).

Model parameterization is used to create ERA Interim clouds, however, changes in net radiation at the TOA are satisfactory compared to satellite data (Allan 2011). The deficiency of changes in the optical depth of aerosols seems rational based on the correlation with surface temperature and previous analysis (Allan 2009). Although clouds drive to the tropical tropospheric heating and the cooling of the atmospheric column for stratocumulus regions and higher latitudes, their atmospheric energy budget is very weak as explained by John et al. (2009). This statement agrees with the simple global mean, zero-dimensional, climate model where the value of ratio R for cloud albedo equals to one and thus its atmospheric forcing tends to zero.

4.1.3 Comparison of Observations with Results

The global mean temperature anomaly of observations and simple climate model including all RF agents are illustrated in Figure 4.2. As shown, the model mostly agrees with the observations (with a correlation coefficient³ $r = 0.85$). Vital events from 1990 to 2010 show agreement between the models and the observations, such as the cooling in 1992 following the strong eruption of Mt. Pinatubo in 1991 and the rapid increase of the surface temperature from 1994-2000.

However, the observed cooling over the last few years is not picked up on by the simple model. Also, the model does not replicate the peak shown in observations occurring in 1940 – implying that there possibly a RF which is neglected from the simple climate model. It is thought that the peak in observed temperatures in the early 1940s could be a result of changes in ship measurements of sea surface temperature during the World War II (Folland and Parker, 1995), which were undocumented

³ The quantity r , called the linear correlation coefficient, measures the strength and the direction of a linear relationship between two variables.

at the time and caused an instrumental artefact. This would mean that the uncertainty is not in the model but in the accuracy of measurements taken. Uncertainties in the observations due to heterogeneous data such as this may explain why the model is not fitting the observed temperature points as closely as it is expected.

It is clear that some RFs are more important in explaining the observed temperature record than others. Solar forcing contributes slightly to the warming but have very little effect on the shape of the model as a whole. The volcanic forcing is significant when analysing the shape of the oscillating observations, especially in the period 1850 to 1880; however they do not explain the warming at the end of the century. This warming is thoroughly evaluated by the well-mixed GHGs and anthropogenic forcings. The model run with volcanic forcing often drops much more steeply than the observations, indicating that there is too much weighting given to this RF in the model. This subsequently causes the model to incompetently match up with the observations (Figure 4.2). The sulphate cloud albedo forcing was shown to have little effect on the model, but due to its ambiguous nature this could mean that the model does not simulate it realistically.

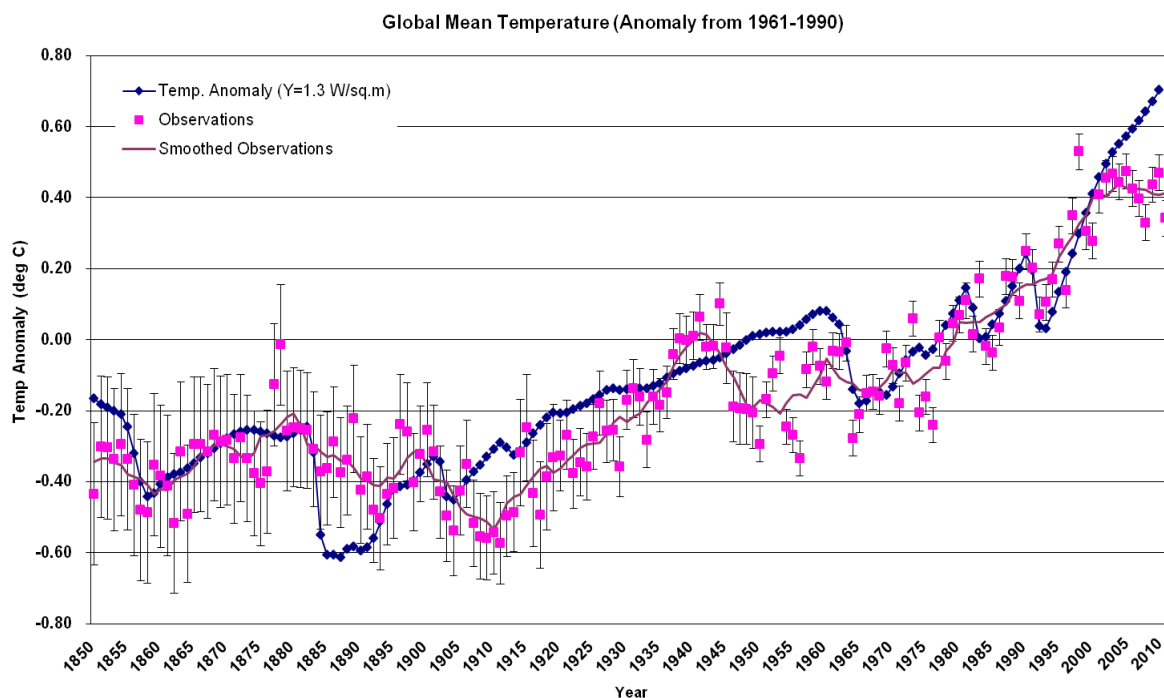


Figure 4.2: Global mean temperature anomaly of observations and model run with all forcings together. Temperature anomalies are relative to 1961-1990.

In reference to section 3.4, the negative RFs of volcanic eruptions and scattering aerosols cause pronounced changes in global surface air temperature (slow component of climate change). Therefore, the decrease of surface temperature cools down the atmospheric temperature, trying to conserve moist adiabats. This effect leads to the reduction of precipitation. On the other hand, the enhanced positive RFs of absorbing aerosols and GHGs, as mentioned in Section 3.1 and 3.2, lead to the increase in global mean-precipitation. Comparing the simple climate model with the observations from 1990 to 2010, it is noticeable that the climate model represents an increase of radiative cooling (Figure 3.11), a result that does not agree with the observations (Figure 4.1c).

Nevertheless, the decrease in global mean precipitation rate computed by the simple climate model agrees with the observations which present a negative trend in precipitation rate up until 2005 followed by a considerable increase (Figure 4.1b). Reasonably the results, produced by the simple climate model, will not include the continuous oscillations illustrated in observations, as a zero-dimensional climate model does not involve detailed description of physical processes containing their equations as complex models do.

4.2 Temperature and precipitation response using complex climate models

In this section, the time series of global mean temperature anomaly and precipitation rate, using complex climate models are presented. The ten complex models that are used include BCC, CanESM2, NorESM1 M, MRI CGCM3, MPI ESM LR, MIROC5, IPSL CM5A LR, HadGEM2, CNRM CM5 and CCSM4 (Taylor et al., 2012). Each model provides “historical” simulations (prescribed past changes in RF via emissions) including data for precipitation rate and temperature. Estimating the average temperature from 1961 to 1990 and subtracting this from the given temperature values, the temperature anomalies for each complex climate model are computed. Afterwards, the average values from all models for both temperature anomalies and global-mean precipitation changes are gauged and are illustrated in Figures 4.3 and 4.4, compared to the observations and results from simple climate model.

4.2.1 Global-mean temperature anomaly

The observed global mean temperature anomalies and those produced by the simple and complex climate models including all RF agents are shown in Figure 4.3. Arguably, there is a good agreement between them with a correlation coefficient $r=0.86$. Major events from 1850 to 2010 showed correspondence between the simple and the complex climate models, such as the cooling in 1883

and 1992 following the strong volcanic eruptions of Krakatoa in 1883 and Mt. Pinatubo in 1991. Additionally, both simple and complex climate models demonstrate a significant enhancement of the surface temperature anomalies from 1994-2005.

Although major events are well-demonstrated, neither simple nor complex models illustrate the observed flat ΔT from 2000–2005. Besides, the continuous oscillations from 1915 to 1960 illustrated by the complex climate models are not presented in the simple climate model, as the complex climate models contain comprehensive description of physical processes including their equations. In addition, complex climate models may include more RF terms which are not determined in the simple climate model which is used in this project.

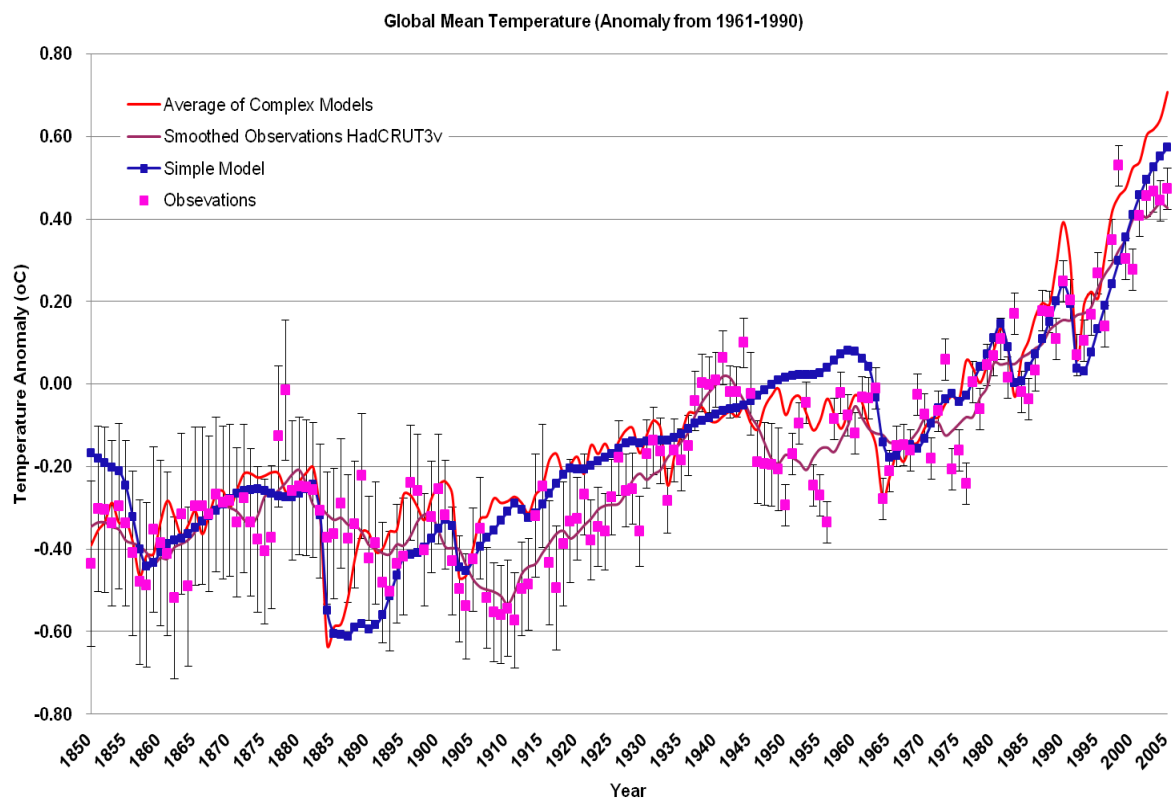


Figure 4.3: Comparison of global mean temperature anomaly time series for observations, simple climate model and complex climate models. The short-time minima are caused by volcanic sulphates and they agree with the literature as it can be observed that their effect lasts 2-3 years. The increase of temperature anomaly the last decades (after 1960) is caused by the GHGs and it would be more rapid if the scattering aerosols were not taken into account.

Table 3: Demonstration of correlation coefficient between observations, simple climate model and complex climate models for the global mean temperature anomaly

	Correlation Coefficient (r)
Observations – Simple Climate Model	0.85
Observations – Complex Climate Model	0.85
Simple C.M – Complex C.Ms	0.84

4.2.2 Global-mean precipitation rate

The time series of global mean precipitation changes simulated by simple and complex climate models are illustrated in Figure 4.4. The correlation coefficient is $r=0.75$, representing a good agreement between simple and complex models. Both of them represent sudden, rapid, and short-lived (2-3 years) reductions of precipitation during the strong volcanic eruptions and a rapid increase since 1993 (after the eruption of Mt. Pinatubo). The increase after 1993 is associated with the rapid growth of climate change mechanisms that largely force the climate through the absorption of solar radiation and essentially perturb precipitation through changes in global surface air temperature.

Comparing the results to the observations from 1985 to 2005, the average of complex climate models mostly agrees with the SSM/I, while the simple climate model displays substantial differences. These differences were not caused only because the model is highly simplified but generated also by other factors. Firstly, the observational data are subject to errors of non-climatic sources resulting from data gaps, random error, urbanization, and change in observational practices and SST bias corrections (Folland et al., 2001). Other sources of errors such as computational errors in averaging the point data and the technique used to minimize the errors and the remaining uncertainties were also discussed. Additionally, a random internal variability of climate can also lead to these differences. Secondly, there are a number of uncertainties in the RFs, especially in the indirect effect of cloud albedo. Thirdly, there are possible errors due to the fixed values of model parameters, such as hydrological sensitivity, feedback parameter and ratio R can cause errors between simple and complex models.

For example, if the hydrological sensitivity for only the slow components of climate change is increased to 3%/K, it can be observed that all major events and the overall positive trend, produced by the complex models and the observations, is also determined by the simple climate model.

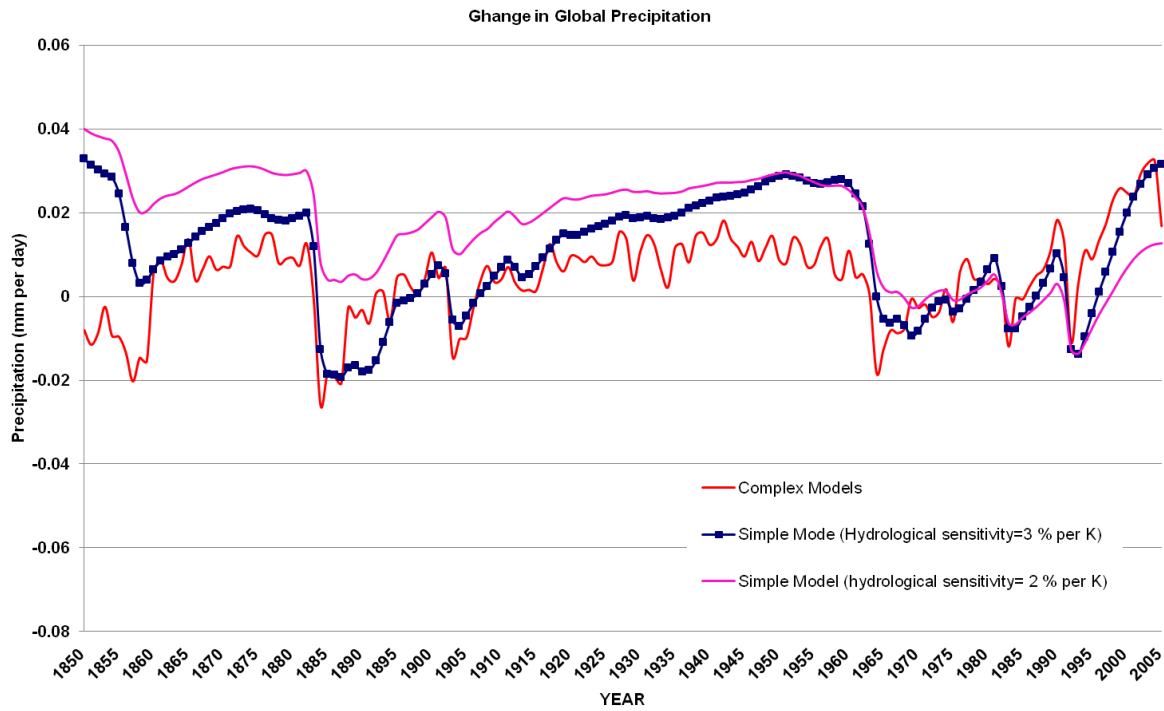


Figure 4.4: Time series of the global-mean precipitation rate using complex climate models. The global mean-precipitation generally increased during the last decades as the atmospheric forcing (fast component of climate change) increased slower than the radiative cooling of the atmosphere (slow component of climate change). Further temporary diminutions (about 2 to 3 years) of global mean-precipitation are related to the occasional volcanic eruptions.

Chapter 5: Conclusions and Further Work

5.1 Conclusions

The precipitation response and the relationship to RF have been examined in relation to a variety of climate change mechanisms. Two different timescales responses have been defined; a fast atmospheric component relative to the RF and a slower component that scales with changes in the surface temperature. The numerical simulations are established by a simple, zero-dimensional climate model following the methodology of Hansen et al. (1981), including a mixed-layer ocean coupled to a deep ocean by diffusion. The simple model uses time series for both anthropogenic and natural forcings at the TOA from well-mixed greenhouse gases, both absorbing and scattering aerosols, volcanic aerosols, and solar irradiance.

5.1.1 Experiments

In running this simple climate model, all the RF agents have been used in order to establish the major forcings that determine the global mean precipitation changes. By running the simple climate model, it can be observed that the positive temperature anomalies have increased during the most recent four decades. However, these positive temperature anomalies are occasionally perturbed by some strong, short-lived (on a scale of 2-3 years) decreasing temperature anomaly trends. In addition, a discernible periodic motion is noticed between 1915 and 1960, whilst the global mean precipitation rate is reduced. This is because precipitation is dominated by the response to global surface temperature change. Further temporary reductions of precipitation rate are related to the occasional decreasing temperature anomaly trends. The simple climate model shows that:

- During the industrial era, the concentrations of well-mixed GHGs rose, leading to a positive RF at the TOA. The enhancement of RF causes an increase in global surface-air-temperature anomalies (0.8°C). The atmospheric component illustrates a near-exponential increase reaching 2 Wm^{-2} . However, the slow response to global temperature changes increased more rapidly than the quick atmospheric response to the RFs, resulting in the increase in precipitation rate.
- The negative RF of scattering aerosols at the TOA decreases surface temperature. The fast atmospheric component is neglected because the atmosphere is largely transparent to the scattering aerosols RFs. Therefore, the slow response to global temperature change suppresses the precipitation rate.

- The increase of absorbing aerosols concentration causes an enhanced positive RF at the TOA. This leads to a small increase in surface temperature anomaly (0.25°C). However, for absorbing aerosols the fast atmospheric component is sufficiently large, reaching 0.80 Wm^{-2} . Therefore, the fast atmospheric component is larger than the slow response to global surface temperature anomalies. According to Eq.9, the precipitation response is of opposite sign to both fast and slow component of precipitation.
- A slight increase in solar irradiance has been observed since the late 1970s, determining an insignificant atmospheric forcing with maximum value of 0.05 Wm^{-2} . However, the solar forcing is important in explaining some of the observed warming. Therefore, the slow response to global temperature change is larger than the fast atmospheric component, enhancing the precipitation rate.
- Volcanic eruptions cause large negative RF at the TOA, leading to sudden decreasing temperature anomaly trends (for example -0.20°C in 1991). The atmosphere is largely transparent to the RF of volcanic eruptions. Therefore, the precipitation rate is dominated by the slow response to global temperature change. This leads to a reduction in precipitation rate.

Typically, the climate change mechanisms that perturb Earth's energy budget through absorption of solar radiation in the troposphere, such as GHGs, are dominated by the slow component of precipitation. However, the fast atmospheric component of black carbon is substantial, suppressing precipitation rate. Also it is shown that climate change mechanisms which drive climate through the scattering of solar radiation for example, scattering aerosols, perturb the precipitation rate through reductions in the global surface temperature. Consequently, this suppresses precipitation rate.

In comparing the results to the complex models, there is a good agreement between them (correlation coefficient is of the order 0.7 - 0.8). Some RFs are more important in explaining the observed temperature record and precipitation rate than others. One of the most critical RFs is the volcanic eruptions which explain the sudden short-lived reductions in global precipitation rate. In addition, the major factor which determines the enhancement of both fast and slow components of precipitation is the rapid increase of well-mixed GHGs concentrations.

However, the increase in precipitation rate seen in the last two decades, produced by the simple climate model is not as large as the precipitation rate produced by the complex models. Consequently, further changes are required in this simple climate model. It has been demonstrated that by increasing the hydrological sensitivity, there is a better agreement with the complex climate

models. It is reasonable that the results given by the simple climate model will not include the continuous oscillations illustrated by the complex models. This is because a zero-dimensional climate model does not involve detailed description of physical processes containing their equations as complex models do.

5.1.3 Further experiments to explore and understand the uncertainty of the simple model

Two further experiments were conducted which involved changing the value for the ratio R_{BC} as evaluated by Andrews et al. (2010) and the feedback parameter:

- By negatively increasing the value of R_{BC} ($R_{BC} < -1.5$), the RF of black carbon (BC) at the TOA and the temperature anomaly has to be increased. This is not feasible as the values of all of the RFs at the TOA are fixed and therefore cannot be increased. The atmospheric forcing is increased tending to suppress the precipitation rate. Nevertheless, the increase of fast atmospheric response is more rapid than the increase of slow response, suppressing the precipitation rate. The complex models produce an increase in precipitation rate in the last two decades; if $R_{BC} > -1.5$, the global mean precipitation rate produced by the simple climate model would have a better agreement with the outcome of complex climate models.
- An increase in feedback parameter tends to balance the energy budget of the atmosphere and to diminish the changes of global-mean precipitation rate. Also a reduction of feedback parameter tends to cause further perturbation to the energy budget of the atmosphere, leading to the enhancement of global mean precipitation rate.

In conclusion, the possible parameters that could be changed in order to improve the correspondence with the complex models are:

1. The increase of ratio R_{BC} ($R_{BC} > -1.5$)
2. The increase of feedback parameter Y ($1.3 \text{ Wm}^{-2} < Y < 3.3 \text{ Wm}^{-2}$)
3. The increase of hydrological parameter ($\kappa > 2 \text{ \%K}^{-1}$)

5.2 Future Work

Areas of future research which would improve the understanding of the accuracy of changes in precipitation rate produced by the simple climate model are:

- a) An experiment changing the heat capacity of the ocean, the diffusion or any other natural variable could demonstrate how well the model describes the natural variability of the climate system. It would be beneficial to further test the accuracy of the radiative constraint in the free-atmosphere, storing the necessary radiative fluxes in the climate model (O’Gorman et al., 2011).
- b) A hierarchy of complexity for climate models can be created by comparing different complex and simple climate models. Also a high complexity model can be run in order to be compared with the different results produced by the simple climate model.
- c) Finally a future scenario can be created where future changes in precipitation will be represented.
- d) Further research is needed to estimate the accuracy of the ratio R values (Andrews et al., 2010) and to constrain more realistic values of RFs. This could be succeeded by using recently available simulations from the Coupled Model Intercomparison Project phase 5.

Chapter 6: References

6.1 Bibliography

Adler, R. F., C. Kidd, G. Petty, M. Morrissey, and H. Goodman, 2001: Intercomparison of global precipitation products: The third Precipitation Intercomparison Project (PIP-3). *Bull. Amer. Meteor. Soc.*, **82**, 1377–1396.

Adler, D.S., Bar-Yosef, O., Belfer-Cohen, A., Tushabramishvili, N., Boaretto, E., Mercier, N., Valladas, H., Rink, W.J., 2008: Dating the demise: neandertal extinction and the establishment of modern humans in the southern Caucasus. In: Adler, D.S., Joris, O. (Eds.), *Setting the Record Straight: Toward a Systematic Chronological Understanding of the Middle to Upper Paleolithic Boundary in Eurasia*. *J. Hum. Evol.* 55, 817–833.

Allan, R.P. and John, V.O., 2009: Monitoring changes in precipitation and radiative energy using satellite data and climate models. Proceedings of the 2009 EUMETSAT Meteorological Satellite Conference, P.55. S6, 37. ISSN 1011-3932.

Allan, RP, 2011: Combining satellite data and models to estimate cloud radiative effect at the surface and in the atmosphere. *Meteorol Appl*, **18**:324–333.

Allen, M. R. and Ingram, W. J., 2002: Constraints on future changes in climate and the hydrologic cycle. *Nature*, **419**, 224–232.

Ammann, C. M., G. A. Meehl, W. M. Washington, and C. S. Zender, 2003: A monthly and latitudinally varying volcanic forcing dataset in simulations of 20th century climate. *Geophys. Res. Lett.*, **30(12)**, 1657, doi:10.1029/2003GL016875.

Anagnostou, E.N., M.N. Anagnostou, A. Kruger, W.F. Krajewski, and B. Miriovsky, 2004: High resolution rainfall estimation from X-band polarimetric radar measurements. *Journal of Hydrometeorology*, **43(1)**, 106-118.

Andrews, Timothy, Piers M. Forster, Jonathan M. Gregory, 2009: A Surface Energy Perspective on Climate Change. *J. Climate*, **22**, 2557–2570, doi: 10.1175/2008JCLI2759.1.

- Andrews, T., P. M. Forster, O. Boucher, N. Bellouin and A. Jones, 2010: Precipitation, radiative forcing and global temperature change. *Geophys. Res. Lett.*, **37**, L14701, doi: 10.1029/2010GL043991.
- Arkin, P. A., T. M. Smith, M. R. P. Sapiano, and J. Janowiak, 2010: The observed sensitivity of the global hydrological cycle to changes in surface temperature. *Environ. Res. Lett.*, **5**, 035201, doi:10.1088/1748-9326/5/3/035201.
- Bala, G., K. Caldeira, and R. Nemani, 2009: Fast versus slow response in climate change: implications for the global hydrological cycle. *Clim.Dyn.*, doi:10.1007/s00382-009-0583-y.
- Bates, B.C., Z.W. Kundzewicz, S. Wu and J.P. Palutikof, Eds., 2008: Climate Change and Water. Technical Paper of the Intergovernmental Panel on Climate Change, IPCC Secretariat, Geneva, 210 pp.
- Bingen, B., Griffin, W.L. and Saeed, A., 2004: Detrital zircon signature of Baltica during the Neoproterozoic: LA-ICP-MS U-Pb and Lu-Hf study of the Lower Allochthon of SE Norway and implications (Abstract). *GFF*, **126**, 78.
- Bony, Sandrine, and Coauthors, 2006: How Well Do We Understand and Evaluate Climate Change Feedback Processes?. *J. Climate*, **19**, 3445–3482, doi: 10.1175/JCLI3819.1.
- Brohan, P., J.J. Kennedy, I. Harris, S.F.B. Tett and P.D. Jones, 2006: Uncertainty estimates in regional and global observed temperature changes: a new dataset from 1850. *J. Geophysical Research* **111**, D12106, doi:10.1029/2005JD006548.
- Collins, W.D., V. Ramaswamy, M.D. Schwarzkopf, Y. Sun, R.W. Portmann, Q. Fu, S.E.B. Casanova, J.-L. Dufresne, D.W. Fillmore, P.M.D. Forster, V.Y. Galin, L.K. Gohar, W.J. Ingram, D.P. Kratz, M.-P. Lefebvre, J. Li, P. Marquet, V. Oinas, Y. Tsushima, T. Uchiyama, and W.Y. Zhong, 2006: Radiative forcing by well-mixed greenhouse gases: Estimates from climate models in the Intergovernmental Panel on Climate Change (IPCC) Fourth Assessment Report (AR4). *J. Geophys. Res.*, **111**, D14317, doi:10.1029/2005JD006713.
- Dee, D.P., and Coauthors, 2011a: The ERA-Interim reanalysis: Configuration and performance of the data assimilation system. *Quart. J. Roy. Meteor. Soc.*, **137**, 553–597.
- Dong, B., J. M. Gregory, and R. T. Sutton, 2009: Understanding land-sea warming contrast in response to increasing greenhouse gases. Part I: Transient adjustment, *J. Clim.*, **22**, 3079–3097, doi:10.1175/2009JCLI2652.1.

Folland, C.K., and D.E. Parker, 1995: Correction of instrumental biases in historical sea surface temperature data. *Q. J. R. Meteorol. Soc.*, **121**, 319-367.

Forster, P., V. Ramaswamy, P. Artaxo, T. Berntsen, R. Betts, D.W. Fahey, J. Haywood, J. Lean, D.C. Lowe, G. Myhre, J. Nganga, R. Prinn, G. Raga, M. Schulz and R. Van Dorland, 2007: Changes in Atmospheric Constituents and in Radiative Forcing. In: *Climate Change 2007: The Physical Science Basis. Contribution of Working Group I to the Fourth Assessment Report of the Intergovernmental Panel on Climate Change* [Solomon, S., D. Qin, M. Manning, Z. Chen, M. Marquis, K.B. Averyt, M. Tignor and H.L. Miller (eds.)]. Cambridge University Press, Cambridge, United Kingdom and New York, NY, USA

Haigh, J. D., 1994: The role of stratospheric ozone in modulating the solar radiative forcing of climate. *Nature*, **370**, 544–546.

Hansen, J., D. Johnson, A. Lacis, S. Lebedeff, P. Lee, D. Rind, and G. Russell, 1981: Climate impact of increasing atmospheric carbon dioxide. *Science*, **213**, 957-966, doi:10.1126/science.213.4511.957.

Hansen, J., Mki. Sato, and R. Ruedy, 1997: Radiative forcing and climate response. *J. Geophys. Res.*, **102**, 6831-6864, doi:10.1029/96JD03436.

Hansen, J., Mki. Sato, L. Nazarenko, R. Ruedy, A. Lacis, D. Koch, I. Tegen, T. Hall, D. Shindell, B. Santer, P. Stone, T. Novakov, L. Thomason, R. Wang, Y. Wang, D. Jacob, S. Hollandsworth, L. Bishop, J. Logan, A. Thompson, R. Stolarski, J. Lean, R. Willson, S. Levitus, J. Antonov, N. Rayner, D. Parker, and J. Christy, 2002: Climate forcings in Goddard Institute for Space Studies SI2000 simulations. *J. Geophys. Res.*, **107**, no. D18, 4347, doi:10.1029/2001JD001143.

Hansen, J. & Sato, M., 2004: Greenhouse gas growth rates.. *Proc. Natl Acad. Sci. USA*, **101**, 16 109–16 114, doi:10.1073/pnas.0406982101)

Hansen, J., Mki. Sato, P. Kharecha, G. Russell, D.W. Lea, and M. Siddall, 2007: Climate change and trace gases. *Phil. Trans. Royal. Soc. A*, **365**, 1925-1954, doi:10.1098/rsta.2007.2052.

Hansen, J., Mki. Sato, R. Ruedy, P. Kharecha, A. Lacis, R.L. Miller, L. Nazarenko, K. Lo, G.A. Schmidt, G. Russell, I. Aleinov, S. Bauer, E. Baum, B. Cairns, V. Canuto, M. Chandler, Y. Cheng, A. Cohen, A. Del Genio, G. Faluvegi, E. Fleming, A. Friend, T. Hall, C. Jackman, J. Jonas, M. Kelley, N.Y. Kiang, D. Koch, G. Labow, J. Lerner, S. Menon, T. Novakov, V. Oinas, J.P. Perlwitz, Ju. Perlwitz, D. Rind, A. Romanou, R. Schmunk, D. Shindell, P. Stone, S. Sun, D. Streets, N. Tausnev, D. Thresher, N. Unger, M. Yao, and S. Zhang, 2007: Climate simulations for 1880-2003 with GISS modelE. *Clim. Dynam.*, **29**, 661-696, doi:10.1007/s00382-007-0255-8.

- Harvey, L.D.D., 2000: *Global warming: The hard science*. Prentice Hall, Harlow, UK, 336pp.
- Haywood, J. M., et al., 2010: Observations of the eruption of the Sarychev volcano and simulations using the HadGEM2 climate model. *J. Geophys. Res.*, **115**, D21212, doi:10.1029/2010JD014447.
- Hegerl, G.C., F. W. Zwiers, P. Braconnot, N.P. Gillett, Y. Luo, J.A. Marengo Orsini, N. Nicholls, J.E. Penner and P.A. Stott, 2007: Understanding and Attributing Climate Change. In: *Climate Change 2007: The Physical Science Basis. Contribution of Working Group I to the Fourth Assessment Report of the Intergovernmental Panel on Climate Change* [Solomon, S., D. Qin, M. Manning, Z. Chen, M. Marquis, K.B. Averyt, M. Tignor and H.L. Miller (eds.)]. Cambridge University Press, Cambridge, United Kingdom and New York, NY, USA.
- Held, I. M. & Soden, B. J., 2006: Robust responses of the hydrological cycle to global warming. *J. Clim.* **19**, 5686–5699
- Huffman, G.J., R.F. Adler, D.T. Bolvin, G. Gu, 2009: Improving the Global Precipitation Record: GPCP Version 2.1. *Geophys. Res. Lett.*, **36**, L17808, doi:10.1029/2009GL040000.
- IPCC, 1990: *Climate Change: The Intergovernmental Panel on Climate Change Scientific Assessment* [Houghton, J.T., G.J. Jenkins, and J.J. Ephraums (eds.)]. Cambridge University Press, Cambridge, United Kingdom and New York, NY, USA, 365 pp
- IPCC, 2001: *Climate Change 2001: The Scientific Basis. Contribution of Working Group I to the Third Assessment Report of the Intergovernmental Panel on Climate Change* [Houghton, J.T., Y. Ding, D.J. Griggs, M. Noguer, P.J. van der Linden, X. Dai, K. Maskell, and C.A. Johnson (eds.)]. Cambridge University Press, Cambridge, United Kingdom and New York, NY, USA, 881pp.
- IPCC, 2007: *Climate Change 2007: The Physical Science Basis. Contribution of Working Group I to the Fourth Assessment Report of the Intergovernmental Panel on Climate Change* [Solomon, S., D. Qin, M. Manning, Z. Chen, M. Marquis, K.B. Averyt, M. Tignor and H.L. Miller (eds.)]. Cambridge University Press, Cambridge, United Kingdom and New York, NY, USA, 996 pp.
- Kiehl, J. T., 2007: Twentieth century climate model response and climate sensitivity, *Geophys. Res. Lett.*, **34**, L22710, doi:10.1029/2007GL031383.
- Koch, D., 2001: Transport and direct radiative forcing of carbonaceous and sulfate aerosols in the GISS GCM. *J. Geophys. Res.*, **106**, 20311–20332, doi:10.1029/2001JD900038.
- Lacis, A.A, G.A. Schmidt, D. Rind, and R.A. Ruedy, 2010: Atmospheric CO₂: Principal control knob governing Earth's temperature. *Science*, **330**, 356–359, doi:10.1126/science.1190653.

Lambert, F. H., and M. J. Webb, 2008: Dependency of global mean precipitation on surface temperature, *Geophys. Res. Lett.*, **35**, L16706, doi:10.1029/2008GL034838.

Le Treut, H., R. Somerville, U. Cubasch, Y. Ding, C. Mauritzen, A. Mokssit, T. Peterson and M. Prather, 2007: Historical Overview of Climate Change. In: *Climate Change 2007: The Physical Science Basis. Contribution of Working Group I to the Fourth Assessment Report of the Intergovernmental Panel on Climate Change* [Solomon, S., D. Qin, M. Manning, Z. Chen, M. Marquis, K.B. Averyt, M. Tignor and H.L. Miller (eds.)]. Cambridge University Press, Cambridge, United Kingdom and New York, NY, USA.

Lean, J., 2000: Evolution of the Sun's spectral irradiance since the Maunder Minimum. *Geophys. Res. Lett.*, **27**, 2425 – 2428.

Lean, J.L., Y.M. Wang, and N.R. Sheeley, 2002: The effect of increasing solar activity on the Sun's total and open magnetic flux during multiple cycles: Implications for solar forcing of climate. *Geophys. Res. Lett.*, **29(24)**, 2224, doi:10.1029/2002GL015880.

Li G, Ren B, Yang C, Zheng J, 2011: Revisiting the trend of the tropical and subtropical Pacific surface latent heat flux during 1977–2006. *J Geophys Res* 116:D10115

Loeb, N. G., and Coauthors, 2009: Toward optimal closure of the Earth's top-of-atmosphere radiation budget. *J. Climate*, in press.

Loeb, N.G., J.M. Lyman, G.C. Johnson, R.P. Allan, D.R. Doelling, T. Wong, B.J. Soden, and G.L. Stephens, 2012: Observed changes in top-of-the-atmosphere radiation and upper-ocean heating consistent within uncertainty. *Nature Geosciences*, doi:10.1038/NGEO1375.

Lohmann, U., and J. Feichter, 2005: Global indirect aerosol effects: A review. *Atmos. Chem. Phys.*, **5**, 715–737.

Menon, S., A.D. Del Genio, D. Koch and G. Tselioudis, 2002: GCM simulations of the aerosol indirect effect: Sensitivity to cloud parameterization and aerosol burden. *J. Atmos. Sci.*, **59**, 692-713.

Min, S. K. et al. Human contribution to more-intense precipitation extremes, 2011: *Nature*, **470**, 378–381.

Ming, Y., V. Ramaswamy, and G. Persad, 2010: Two opposing effects of absorbing aerosols on global-mean precipitation, *Geophys. Res. Lett.*, **37**, L13701, doi:10.1029/2010GL042895.

Minnis, Patrick, J. Kirk Ayers, Rabindra Palikonda, Dung Phan, 2004: Contrails, Cirrus Trends, and Climate. *J. Climate*, **17**, 1671–1685, doi:

- Mitchell, J. F. B. and Warrilow, D. A., 1987: Summer Dryness in Northern Mid-latitudes Due To Increased CO₂. *Nature*, **330**, 238–240.
- Montzka, S. A., et al., 1999: Present and future trends in the atmospheric burden of ozone-depleting halogens. *Nature*, **398**, 690 – 694.
- Novakov, T., V. Ramanathan, J.E. Hansen, T.W. Kirchstetter, Mki. Sato, J.E. Sinton, and J.A. Satahye, 2003: Large historical changes of fossil-fuel black carbon aerosols. *Geophys. Res. Lett.*, **30**, no. 6, 1324, doi:10.1029/2002GL016345.
- O'Gorman, P. A., R. P. Allan, M. P. Byrne, and M. Previdi, 2011: Energetic constraints on precipitation under climate change. *Surv. Geophys.*, doi:10.1007/s10712-011-9159-6.
- Penner, I. K., Kobel, M., & Opwis, K., 2006: BrainStim – A recently developed tool to train different aspects of working memory. *Proceedings of the INS/GNP Conference*, 17–18.
- Quaas, J. and Boucher, O., 2005: Constraining the first aerosol indirect radiative forcing in the LMDZ GCM using POLDER and MODIS satellite data. *Geophys. Res. Lett.*, **32**, L17814, 20, doi:10.1029/2005GL023850.
- Ramanathan, V., 1981: The role of ocean–atmosphere interactions in the CO₂ climate problem. *J. Atmos. Sci.*, **38**, 918–30.
- Ramanathan, V., Crutzen, P. J., Kiehl, J. T., and Rosenfeld, D., 2001a: Aerosols, climate and the hydrological cycle, *Science*, **294**, 2119–2124.
- Randel, W.J., and F. Wu, 1999: Cooling of the Arctic and Antarctic polar stratosphere due to ozone depletion. *J. Climate*, **12**, 1467-1479.
- Randall, D.A., R.A. Wood, S. Bony, R. Colman, T. Fichet, J. Fyfe, V. Kattsov, A. Pitman, J. Shukla, J. Srinivasan, R.J. Stouffer, A. Sumi and K.E. Taylor, 2007: Climate Models and Their Evaluation. In: *Climate Change 2007: The Physical Science Basis. Contribution of Working Group I to the Fourth Assessment Report of the Intergovernmental Panel on Climate Change* [Solomon, S., D. Qin, M. Manning, Z. Chen, M. Marquis, K.B. Averyt, M. Tignor and H.L. Miller (eds.)]. Cambridge University Press, Cambridge, United Kingdom and New York, NY, USA.
- Raval, A., and V. Ramanathan, 1989: Observational determination of the greenhouse effect. *Nature*, **342**, 758-761.

Robine, J.M., S.L. Cheung, S. Le Roy, H. Van Oyen, C. Griffiths, J.P. Michel, and F.R.Herrmann, 2008: Death toll exceeded 70,000 in Europe during the summer of 2003. *Comptes Rendus Biologies*, **331(2)**, 171-178.

Sato, Mki., J.E. Hansen, M.P. McCormick, and J.B. Pollack, 1993: Stratospheric aerosol optical depths, 1850-1990. *J. Geophys. Res.*, **98**, 22987-22994, doi:10.1029/93JD02553.

Shindell, D.T., G.A. Schmidt, R.L. Miller, and M.E. Mann, 2003: Volcanic and solar forcing of climate change during the preindustrial era. *J. Climate*, **16**, 4094-4107, doi:10.1175/1520-0442(2003)016<4094:VASFOC>2.0.CO;2.

Schmidt, G. A., R. A. Ruedy, R. L. Miller, and A. A. Lacis, 2010: Attribution of the present-day total greenhouse effect. *J. Geophys. Res.*, **115**, D20106, doi: 10.1029/2010JD014287.

Shine, K.P., A. Henderson-Sellers, A. Slingo, 1984: The influence of the spectral response of satellite sensors on estimates of broadband albedo. *Quart. J. R. Met. SOC.*, **110**, pp. 1170-1179

Shindell, D., D. Rind, N. Balachandran, J. Lean, and P. Lonergan, 1999: Solar cycle variability, ozone, and climate. *Science*, **284**, 305-308, doi:10.1126/science.284.5412.305.

Shindell, D.T., G.A. Schmidt, M.E. Mann, D. Rind, and A. Waple, 2001: Solar forcing of regional climate change during the Maunder Minimum. *Science*, **294**, 2149-2152, doi:10.1126/science.1064363.

Shiogama, H., S. Emori, K. Takahashi, T. Nagashima, T. Ogura, T. Nozawa, and T. Takemura, 2010a: Emission scenario dependency of precipitation on global warming in the MIROC3.2 model. *J. Clim.*, **23**, 2404–2417

Stackhouse, P. W., Jr., S. K. Gupta, S. J. Cox, T. Zhang, J. C. Mikovitz, and L. M. Hinkelman, 2011: 24.5-year SRB data set released. *GEWEX News*, **21(1)**, 10–12.

Stephens, Graeme L., Todd D. Ellis, 2008: Controls of Global-Mean Precipitation Increases in Global Warming GCM Experiments. *J. Climate*, **21**, 6141–6155, doi: 10.1175/2008JCLI2144.1.

Stocker, T.F., G.K.C. Clarke, H. LeTreut, R.S. Lindzen, V.P. Meleshko, R.K. Mugara, T.N. Palmer, R.T. Pierrehumbert, P.J. Sellers, K.E. Trenberth, and J. Willebrand, *Physical climate processes and feedbacks, in Climate Change 2001, The Scientific Basis. Contribution of Working Group I to the Third Assessment Report of the Intergovernmental Panel on Climate Change*, edited by J.T. Houghton, Y. Ding, D.J. Griggs, M. Noguer, P.J. van der Linden, X. Dai, K. Maskell, and C.A. Johnson, 417-470. Cambridge University Press, 2001.

- Takahashi, Ken, 2009: Radiative Constraints on the Hydrological Cycle in an Idealized Radiative–Convective Equilibrium Model. *J. Atmos. Sci.*, **66**, 77–91, doi: 10.1175/2008JAS2797.1.
- Tourpali, K., Schuurmans, C., Van Dorland, R., Steil, B., Brühl, C. and Manzini, E., 2005: Solar cycle modulation of the Arctic Oscillation in a chemistry-climate model. *Geophysical Research Letters*, **32(17)**, doi: 10.1029/2005GL023509.
- Trenberth, K. E., J. M. Caron, D. P. Stepaniak, and S. Worley, 2002: Evolution of El Niño Southern Oscillation and global atmospheric surface temperatures. *J. Geophys. Res.*, **107(D8)**, 4065, doi:10.1029/2000JD000298.
- Trenberth, K.E., A. Dai, R. M. Rasmussen, and D. B. Parsons, 2003: The changing character of precipitation. *Bull. Amer. Meteor. Soc.*, **84**, 1205–1217.
- Trenberth, K.E., P.D. Jones, P. Ambenje, R. Bojariu, D. Easterling, A. Klein Tank, D. Parker, F. Rahimzadeh, J.A. Renwick, M. Rusticucci, B. Soden and P. Zhai, 2007. Observations: Surface and Atmospheric Climate Change. In: *Climate Change 2007: The Physical Science Basis. Contribution of Working Group I to the Fourth Assessment Report of the Intergovernmental Panel on Climate Change* [Solomon, S., D. Qin, M. Manning, Z. Chen, M. Marquis, K.B. Averyt, M. Tignor and H.L. Miller (eds.)]. Cambridge University Press, Cambridge, United Kingdom and New York, NY, USA. Page 235-336.
- Trenberth, Kevin E., John T. Fasullo, Jeffrey Kiehl, 2009: Earth's Global Energy Budget. *Bull. Amer. Meteor. Soc.*, **90**, 311–323, doi: 10.1175/2008BAMS2634.1.
- Wild, O., M.J. Prather, and H. Akimoto, 2001: Indirect long-term global radiative cooling from NO_x emissions. *Geophys. Res. Lett.*, **28(9)**, 1719–1722.
- Wentz, F.J., and M. Schabel, 2000: Precise climate monitoring using complementary satellite data sets. *Nature*, **403**, 414–416.
- Wentz, F. J., L. Ricciardulli, K. Hilburn, and C. Mears, 2007: How much more rain will global warming bring?. *Science*, **317**, 233 – 235, doi:10.1126/science.1140746.
- Zelinka, M. D., and D. L. Hartmann 2010: Why is longwave cloud feedback positive?. *J. Geophys. Res.*, **115**, D16117, doi:10.1029/2010JD013817.
- Zhang, Y.-C., W.B. Rossow, A.A. Lacis, V. Oinas, and M.I. Mishchenko, 2004: Calculation of radiative fluxes from the surface to top of atmosphere based on ISCCP and other global data sets: Refinements of the radiative transfer model and the input data. *J. Geophys. Res.*, **109**, D19105, doi:10.1029/2003JD004457.

6.2 Web, Internet or Other Electronic References

NASA, cited 2003: NASA study finds increasing solar trend that can change climate. [Available online at <http://www.nasa.gov/centers/goddard/news/topstory/2003/0313irradiance.html>.]